Developing an Intelligent Transportation Management Center (ITMC) with a Safety Evaluation Focus for Smart Cities

January 2024 | Final Report

SAFE-D
SAFETY THROUGH DISRUPTION

Texas A&M Transportation Institute

San Diego State University
Leadership Starts Here

VIRGINIA TECH TRANSPORTATION INSTITUTE
VIRGINIA TECH

Disclaimer

The contents of this report reflect the views of the authors, who are responsible for the facts and the accuracy of the information presented herein. This document is disseminated in the interest of information exchange. The report is funded, partially or entirely, by a grant from the U.S. Department of Transportation's University Transportation Centers Program. However, the U.S. Government assumes no liability for the contents or use thereof.

TECHNICAL REPORT DOCUMENTATION PAGE

1. Report No. 04-110	2. Government Accession No.	3. Recipient's Catalog No.
4. Title and Subtitle Developing an Intelligent Transportation Management Center (ITMC) with a Safety Evaluation Focus for Smart Cities		5. Report Date January 2024 6. Performing Organization Code:
7. Author(s) Sina Salehipour Arash Jahangiri Christopher P. Paolini Sahar Ghanipoor Machiani Django Bergcollins		8. Performing Organization Report No. Report 04-110
9. Performing Organization Name and Address: Safe-D National UTC San Diego State University		10. Work Unit No. 11. Contract or Grant No. 69A3551747115/Project 04-110
12. Sponsoring Agency Name and Address Office of the Secretary of Transportation (OST) U.S. Department of Transportation (US DOT)		13. Type of Report and Period Final Research Report 04/2019-12/2023 14. Sponsoring Agency Code

15. Supplementary Notes
This project was funded by the Safety through Disruption (Safe-D) National University Transportation Center, a grant from the U.S. Department of Transportation – Office of the Assistant Secretary for Research and Technology, University Transportation Centers Program.

16. Abstract
In the context of smart cities, ensuring transportation safety is a complex task that involves understanding the impact of new technologies, measuring the effectiveness of safety measures, and identifying high-risk locations. However, recent advances in communication and big data analytics have made it possible to address these challenges in a more efficient manner. Traditional transportation management centers (TMCs) are limited in their ability to analyze large amounts of data for safety evaluation. To overcome this limitation, this project aims to develop an intelligent transportation management center (ITMC) that utilizes automated video analysis to assess safety. By leveraging Intelligent Transportation Systems (ITS) technologies and big data analytics, the proposed ITMC can proactively evaluate safety at signalized intersections. Unlike conventional methods that rely on crash data, the ITMC uses safety surrogate measures (SSMs) to identify near-crash situations and calculate proactive risk. In this study, the results obtained from a machine vision model were used along with the Post Encroachment Time (PET) safety surrogate measure (SSM) to assess safety proactively at a selected signalized intersection. The study utilized the latest YOLO series model, YOLOX, for deep learning to detect and classify road users in video frames from four intersection traffic cameras.

17. Key Words Intelligent Transportation Management Center (ITMC), Intelligent Transportation Systems (ITS) Traffic safety, Signalized Intersection, Post encroachment time (PET), Surrogate safety measures (SSM), YOLOX	18. Distribution Statement No restrictions. This document is available to the public through the Safe-D National UTC website, as well as the following repositories: VTechWorks, The National Transportation Library, The Transportation Library, Volpe National Transportation Systems Center, Federal Highway Administration Research Library, and the National Technical Reports Library.

19. Security Classif. (of this report) Unclassified	20. Security Classif. (of this page) Unclassified	21. No. of Pages 20	22. Price $0

Form DOT F 1700.7 (8-72) Reproduction of completed page authorized

Abstract

In the context of smart cities, ensuring transportation safety is a complex task that involves understanding the impact of new technologies, measuring the effectiveness of safety measures, and identifying high-risk locations. However, recent advances in communication and big data analytics have made it possible to address these challenges in a more efficient manner. Traditional transportation management centers (TMCs) are limited in their ability to analyze large amounts of data for safety evaluation. To overcome this limitation, this project aims to develop an intelligent transportation management center (ITMC) that utilizes automated video analysis to assess safety. By leveraging Intelligent Transportation Systems (ITS) technologies and big data analytics, the proposed ITMC can proactively evaluate safety at signalized intersections. Unlike conventional methods that rely on crash data, the ITMC uses safety surrogate measures (SSMs) to identify near-crash situations and calculate proactive risk. In this study, the results obtained from a machine vision model were used along with the Post Encroachment Time (PET) safety surrogate measure (SSM) to assess safety proactively at a selected signalized intersection. The study utilized the latest YOLO series model, YOLOX, for deep learning to detect and classify road users in video frames from four intersection traffic cameras.

Acknowledgements

This project was funded by the Safety through Disruption (Safe-D) National University Transportation Center, a grant from the U.S. Department of Transportation – Office of the Assistant Secretary for Research and Technology, University Transportation Centers Program.

Table of Contents

List of Figures

Introduction

Transportation management centers (TMCs) oversee critical functions such as incident management, traffic signal operations, and road surveillance (*1*). TMCs play a pivotal role in processing real-time data collected from the field, devising response plans, and implementing strategies to effectively manage the transportation network. However, while TMCs assume significant responsibilities in transportation management, safety studies and routine safety evaluations are often not within their purview. This limitation becomes even more evident when considering the findings of several studies (*2*, *3*) that highlight the benefits and importance of integrating safety considerations into transportation system management and optimization.

Despite the significant advancements in Intelligent Transportation Systems (ITS), sensor technology, and artificial intelligence (AI), TMCs still heavily rely on human operators to perform tasks such as incident detection. This reliance on human resources can undermine the efficiency and accuracy of safety-related operations. The integration of sensors and devices into transportation infrastructure, as well as the widespread use of connected vehicles and personal devices, has given rise to a connected environment. This interconnected ecosystem generates a tremendous volume of data from various sources, including cameras, smartphones, and connected vehicle units. The current state of TMCs does not include the necessary capabilities and tools to effectively address the complex and dynamic challenges that arise. This study aims to tackle the aforementioned challenges by developing an Intelligent Transportation Management Center (ITMC) that leverages advanced machine learning algorithms, big data science, and image processing techniques to proactively evaluate safety at signalized intersections.

Because of their design and function, signalized intersections pose a higher risk for accidents than other areas of the road network. In the United States, over 50% of the combined sum of fatal and injury accidents take place either directly at intersections or in their immediate vicinity (*4*). The primary objective of this study is to utilize video footage captured by four traffic cameras at a signalized intersection to collect essential data for proactive safety monitoring, to enhance safety assessment, and to provide valuable insights into transportation planning and decision-making.

To proactively evaluate safety, surrogate safety measures (SSMs) are often utilized to identify near-crash events. Post encroachment time (PET), a popular SSM, was used in this study to conduct proactive safety analysis. Later in this report, the selection of PET as the most suitable proactive measure is discussed. By utilizing deep learning models and analyzing video frames from four surveillance cameras, objects were detected and classified. The computer-vision model outcomes were then used to compute PET as an SSM. Spatiotemporal analysis of near-crashes was also conducted to investigate where and when these critical events are more likely to occur. Spatiotemporal analyses could assist in solving safety problems and could lead us to understand the mechanism of failure at the time of actual crashes. Furthermore, conflicts between different road users (e.g., vehicles, pedestrians, cyclists), violations of traffic rules, and infrastructure-

related issues (e.g., signal timing) were investigated. A spatial analysis was conducted, resulting in a heatmap visualization that highlights areas where critical events occurred. The heatmap provides a visual representation of safety levels, indicating higher risk exposure and potential safety hotspots. Near-crash events were identified at different times of day (peak vs. off-peak hours, weekend vs. weekdays) and at different stages of the traffic light cycle. Analyzing near-crash events during various phases of the traffic signal cycle provides valuable insights into safety risk dynamics at the signalized intersection. The aim is to identify critical stages where conflicts between road users are more likely to occur. Understanding these patterns is essential for implementing proactive safety countermeasures, optimizing signal timings, and enhancing overall intersection safety.

Proactive Safety Evaluation

Traditionally, safety assessment relies on historical crash and exposure data. However, this approach has several shortcomings, such as the requirement for a significant number of crashes to produce credible results due to the rarity of crashes (*5*, *6*). Consequently, the traditional approach is considered reactive since a significant number of crashes need to occur before an action can be taken. Even a long period of time may not produce enough data, especially if a specific crash type is being studied (e.g., a crash between bicyclists making left turns from an intersection approach and the through traffic on the opposite approach). Moreover, historical crash datasets neglect a significant number of unreported crashes and conflicts that happen more often than crashes (*5*, *7*). In addition, changes may occur over long periods of time, such as design improvements and demand variation, that could potentially impact the results of safety evaluations.

The limitations of reactive safety evaluation also reduce the ability to examine the safety effects of recently implemented safety countermeasures. A proactive solution to address this issue is employing SSMs, which can be used to identify potentially dangerous situations (i.e., near-crashes). In many studies (*8*–*10*) researchers have employed SSMs that analyze non-crash traffic conflicts and near-crashes that happen more frequently (*11*). SSMs are numerical measurements used to identify potentially hazardous events that occur in specific locations along a roadway. The concept of using SSMs was first introduced around the 1960s (*12*); however, new advancements in ITS sensor technologies, machine vision methods, and connected vehicle technologies brought further attention to this field. Most SSMs compute the frequency and severity of traffic conflicts and near-crashes and correlate them with the actual corresponding crashes (*13*). SSMs can aid in identification of locations with high crash risk, enable proactive safety assessment of the transportation system, and measure the effectiveness of certain countermeasures.

Near-crash events are situations where drivers must execute rapid evasive maneuvers, such as emergency braking or steering, when faced with a potential crash risk. Drawing on the kinetic data of moving objects (e.g., vehicles), SSMs can be used to proactively identify safety hazards and recommend times and locations to implement safety countermeasures (*14*). Near-crashes and

actual crashes differ in that near-crashes are situations where a potential crash was narrowly avoided, whereas actual crashes involve a collision between two or more objects. Although near-crashes do not cause the same degree of harm, they are still deemed a significant safety concern. The importance of capturing and recording near-crash events lies in their potential to reveal specific safety hazards that could ultimately cause an actual crash. By identifying these hazards early on, it becomes possible to intervene and prevent crashes from occurring. This underscores the significance of having surveillance systems that are capable of recording near-crash events to aid in the analysis of potential incidents and the development of strategies to mitigate risks.

To detect near-crashes at specific locations, data collection is a crucial step. Various methods, such as video cameras (*15*), smartphones (*16*), and roadside light detection and ranging (LiDAR) (*17*), can be employed. One emerging method is computer vision with deep learning algorithms, which analyzes video footage of traffic flows to identify potential safety hazards at intersections. To better understand how near-crashes are identified, different SSMs methods are essential to consider. These methods are categorized into time-based, energy-based, and deceleration-based SSMs (*18*). The following section provides a brief discussion of these methods.

Time-Based SSM

The time-based SSM category is based on the concept that the proximity in time to a potential collision is a key measure of crash risk (*18*). Time-to-collision (TTC) estimates the remaining time before two road users would collide if they maintain their current paths, but its constant speed assumptions limit its real-world applicability (*19–21*). Time-to-accident predicts the time until a crash occurs, considering the speed and distance of involved vehicles during evasive actions (*22*). Time-exposed TTC and time-integrated TTC assess risk based on hazardous driving duration, with time-exposed TTC useful for microscopic simulations but requiring continuous calculation (*23*). PET measures the time from the first vehicle leaving a conflict area until the second vehicle enters the conflict area, providing realistic risk assessments without relying on constant speed assumptions (*18*). Gap time builds on PET's concept and measures the time difference between two vehicles entering the conflict location, though it is applicable only to angle/crossing interactions and no other situations (*24*).

Deceleration-based SSM

Deceleration rate to avoid the crash (DRAC) is a deceleration-based SSM that quantifies the severity of an encounter by assessing a car's deceleration capability to prevent a collision. It computes the minimum braking rate needed to avoid colliding with another vehicle, assuming one vehicle takes evasive action while the other maintains its speed and direction (18). The Crash Potential Index is another SSM that considers a vehicle's maximum deceleration rate (MADR) to indicate the probability of DRAC exceeding the MADR at any moment (25). Distance-based SSMs, often grouped with deceleration-based SSMs, rely on MADR assumptions and include indicators like rear-end collision risk index and Potential Index for Collision with Urgent Deceleration (PICUD) (26–28). However, PICUD has limitations, such as being only applicable

in lane change scenarios and lacking established threshold values. Other distance-based SSMs have also been proposed, such as Proportion of Stopping Distance, Difference of Space Distance and Stopping Distance, and Unsafe Density, that utilize emergency deceleration rates (29–31).

Energy-based SSM

Energy-based SSMs were developed to assess the severity of interactions, going beyond the crash proximity evaluation offered by time and deceleration-based SSMs. Delta V is a prominent energy-based measure, quantifying the change in velocity resulting from a collision between road users, factoring in mass, speed, and collision angle (32). Bagdadi introduced a conflict severity measure that incorporates delta V, time-to-accident, and a maximum average deceleration assumption, evaluating the effectiveness of evasive maneuvers (33). Laureshyn et al. proposed the extended delta V indicator, combining delta V with time and a deceleration constant to estimate collision likelihood and severity (34). Additionally, energy-based SSMs like Crash Index (CAI) and Conflict Index (CFI) incorporate various kinetic energy variables not limited to delta V. CAI employs acceleration, speed, and minimum time to collision to estimate kinetic energy in car-following interactions (35). CFI considers speeds, masses, angles of road users, and PET to evaluate the probability and severity of a collision (36). These energy-based SSMs offer valuable insights into the severity of conflicts, enhancing transportation safety assessments.

Based on the literature review of different SSM methods and our project goal, we decided to use PET. PET has been widely used and is an accepted measure among researchers. It also has some advantages over other measures. One key advantage is its ability to reflect driver behavior without making assumptions about speed, direction, or collision course. This makes it a valuable measure for accurately assessing safety at intersections by considering real-time interactions of road users. PET also takes into account the lateral distance between vehicles, which is a significant factor in lane-changing scenarios. Furthermore, PET is straightforward to implement and its values have a clear interpretation, which makes it suitable for real-world applications.

ITMC System Architecture Development

After discussing potential locations with the City of Chula Vista, a signalized intersection (Broadway and H Street) was identified for the development and installation of the ITMC. This intersection sees a variety of transportation modes and has had a relatively high number of past roadway crashes. The research team arranged for the installation on mast arms and configured four Hikvision DS-2DY3220IW-DE(4) v.B Series 2 MP Compact Outdoor Network IR PTZ Cameras[1] placed on each of the four traffic light masts at the intersection, with each camera facing toward one of the four approaches (Figure 1[a]).

[1] https://us.hikvision.com/en/products/cameras/network-ptz-camera/value-series/ir/upright-pan-tilt/2-mp-compact-outdoor-network-0

(a) (b)

Figure 1. Photos. (a) Hikvision DS-2DY3220IW-DE4 Outdoor PTZ Camera. (b) A mounted traffic camera on an arm mast of the traffic light located at the intersection of H St and Broadway in Chula Vista.

The research team configured each camera to capture continuous 720p (progressive HD) video, at 10 frames/second, of traffic approaching each light. Figure 2 shows an aerial view of all four ITMC camera installations. The yellow callout boxes indicate the HTTP interface port number used to access the web interface on each camera for orientation (PTZ) configuration, followed by the Real Time Streaming Protocol (RTSP) port number used to capture and save video. Videos were captured and saved every hour on the hour in separate Audio Video Interleave (.avi) container files with Motion JPEG (MJPEG) used for video compression. The data collection period spanned nearly one month, from mid-November 2022 to mid-December 2022. The research specifically focused on near-crash events involving vehicles, trucks, bicycles, motorcycles, and pedestrians.

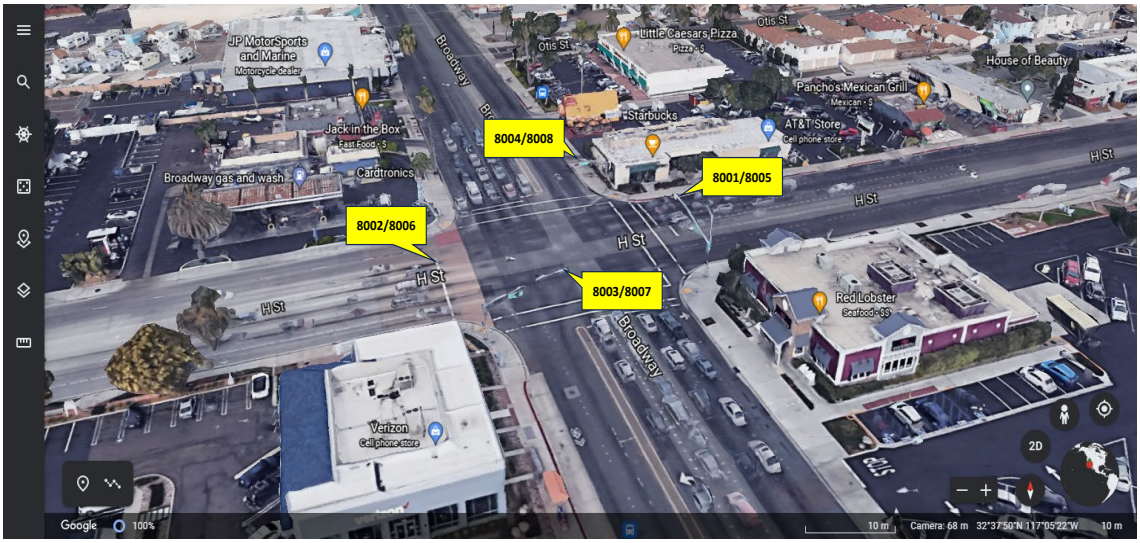

Figure 2. Photo. Aerial view of ITMC camera installations. Yellow callout boxes indicate HTTP interface port number/RTSP port number.

The team installed a Cradlepoint IBR1700 Series Ruggedized Router with an LTE interface to facilitate retrieval of saved video files over a cellular network connection. Each camera was configured to save video files on a separate NVIDIA® Jetson AGX Xavier™ edge device with a USB attached 5 TB hard drive. Videos were copied over a Verizon LTE network to our university GPU server *notos.sdsu.edu* for object detection and post-processing. The IBR1700 router, four Jetson AGXs, and four 5 TB hard drives reside in a sidewalk cabinet in front of the Verizon store

shown in Figure 2. Additional technical details regarding the server, as well as how large amounts of data are processed can be found in Appendix A.

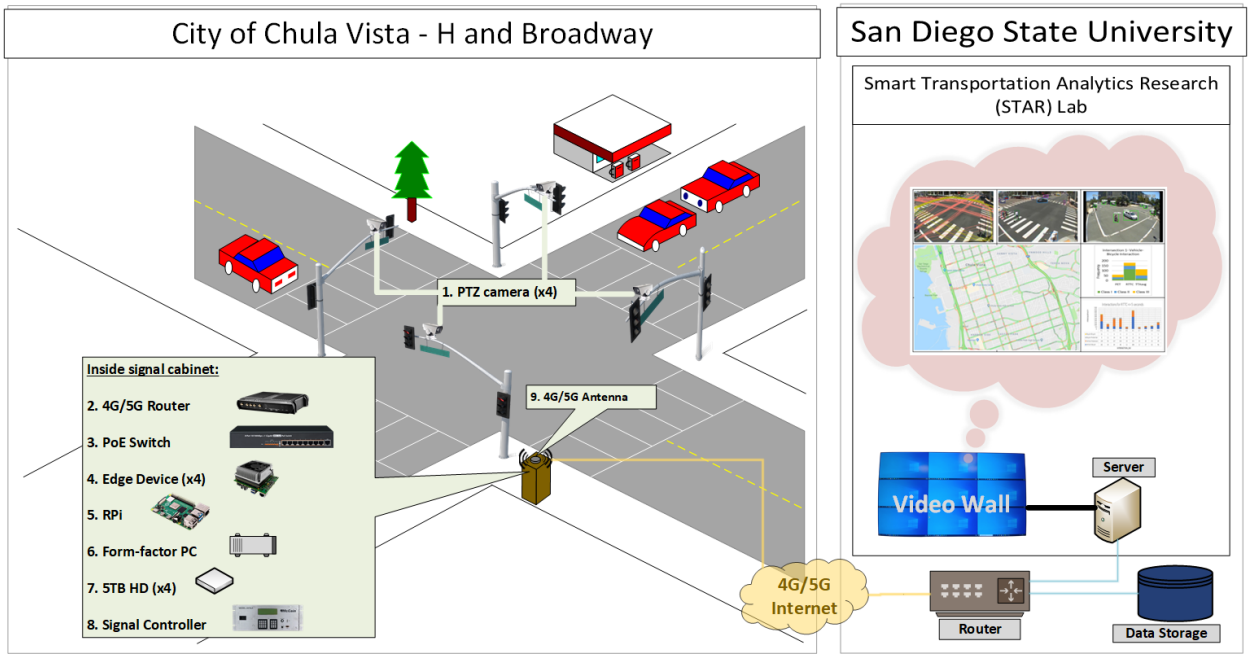

Figure 3. Diagram. Schematic of the intersection of H Street and Broadway in the City of Chula Vista, showing information technology infrastructure installed to support the ITMC project.

Safety Monitoring System Development

A monitoring system was developed to detect and track moving objects (e.g., vehicles) in order to identify near-crash events. This section discusses computer vision models for object detection and classification as well as risk calculations using near-crash event frequency.

Computer Vision Models

Deep learning research has been accelerated by the availability of affordable computer infrastructure, advancements in parallel algorithms, and developments in big data science (*37*). Object detection models are a type of computer vision algorithm used to identify and locate objects within an image or video. These models use deep learning techniques and are trained on large datasets of labeled images to learn patterns and features that can distinguish different objects. Once trained, object detection models can be used in real-world scenarios, making them useful in a wide range of applications such as surveillance, autonomous driving, and object recognition in photos and videos. Popular object detection models include YOLO (You Only Look Once) (*38*), Faster R-CNN (Region-based Convolutional Neural Network) (*39*), and SSD (Single Shot MultiBox Detector) (*40*). In this study, the OpenCV library in Python was utilized for computer vision to perform tasks such as object detection. There are two primary categories of object detection models: two-stage models and one-stage models (*41*). One-stage models integrate the tasks of classification and bounding box detection into one step, resulting in faster performance. Two-stage

detectors first propose the regions of objects using deep features before determining the bounding box and classifying the object. While two-stage detectors are more accurate, they require higher computational resources (*37*). We opted to use one-stage detectors considering the potential real-time future safety applications. In this study, YOLOX, a recent addition to the YOLO series, was employed because of its capacity to strike a balance between speed and accuracy in real-time object detection tasks. YOLOX has surpassed its competitor, YOLOv3, by achieving an average precision of 47.3% on COCO, a dataset comprising 328,000 images utilized for training machine learning models in object detection. (*37*). The COCO dataset consists of real-world images with diverse backgrounds and overlapping objects, making it a good benchmark for evaluating object detection models. Ge et al. (2021) provides a detailed explanation of YOLOX (*42*).

Database Management

We utilized phpMyAdmin to create a MySQL database. phpMyAdmin is a free and open-source administration tool for managing MySQL databases. Each object in our dataset was assigned a unique ID, and data such as object ID, time, block ID, and object name (mode) were recorded in real-time to a MySQL table. This data was collected by tracking the center point of each object's bounding box as it crossed the boundary line of each block. Additionally, the same data was stored in a CSV file for monitoring and debugging purposes. An example of the data stored in both CSV and MySQL formats for a few objects is provided in Appendix B.

Risk Calculation

The computer vision models discussed earlier were utilized to count the number of road users (vehicles, bicycles, pedestrians) crossing the intersections to estimate exposure. The ITMC makes use of these exposure estimations, as well as the frequency of near-crash events, to estimate a risk measure. A general formula to quantify risk was employed as presented in Equation 1.

$$Risk = \frac{Number\ of\ unsafe\ situations}{Exposure} \qquad \text{Equation 1}$$

The ITMC continuously generates video data from four cameras, producing a huge amount of data to be processed. For spatial safety evaluation, the intersection was divided into multiple blocks as shown in 4(a). Each block was used to calculate the PET value for every interaction among objects that occurs within that block. These blocks were created by extending the traffic lines of the four intersection approaches towards the center of the intersection; thus each block is approximately a square with a side length equal to the traffic lane width. To calculate the PET value for two objects interacting with each other, the difference between the exit time of the first object and the arrival time of the second object was computed, an example of which is demonstrated in Figure 4(b). This calculation was carried out for all 90 blocks, and the results were stored in the MySQL database.

Different thresholds for PET have been used in the past to classify near-crash severity. In Zangenehpour et al., an in-depth examination of interactions between cyclists and turning vehicles facilitated the identification of diverse PET thresholds. Specifically, PET values less than 1.5 s were categorized as highly hazardous interactions, while those ranging from 1.5 to 3 s were

deemed risky. PET values spanning from 3 to 5 s indicated mild interactions, while PET values exceeding 5 s suggested a lack of interaction between cyclists and turning vehicles (*43*). Kumar et al. studied pedestrian conflicts with right-turning vehicles at signalized intersections. They used *k*-means clustering to identify a PET range of 0.48 s to 5.40 s, classified into four severity levels for near-crash incidents, ranging from most serious to least serious conflicts (*44*). Marisamynathan and Vedagiri reported that PET values of ≤ 2 s suggested a high probability of interaction between pedestrians and vehicles within the crosswalk. Conversely, PET values greater than 5.5 s indicated no chance of interaction (*45*). Peesapati et al. examined crashes involving left-turning vehicles and opposing through vehicles at four-leg signalized intersections. Their research identified correlations between crashes and various PET thresholds. The highest correlation was observed for PET values of equal to or less than 1 s, followed by those equal to or less than 2 s and 3 s (*46*). In the present study, five PET thresholds (≤ 5 s; ≤ 4 s; ≤ 3 s; ≤ 2 s; and ≤ 1 s) for identifying critical interactions were used. PET values greater than 5 s were assumed to correspond to events with no interactions. The severity of a near-crash event varies depending on the PET value, and thus event severity can be categorized as "Very dangerous," "Dangerous," "Mild," or "No interaction."

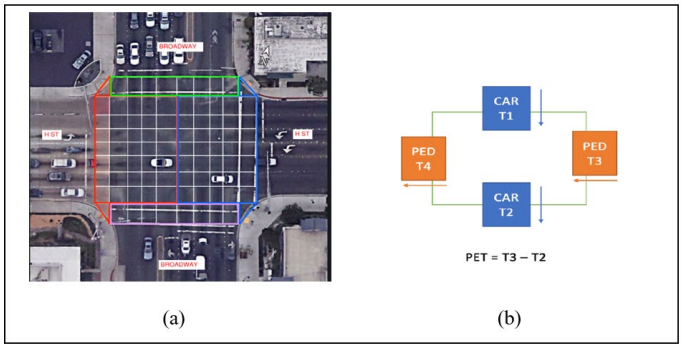

Figure 4. Diagrams. (a) Blocks drawn from the top view, (b) an example of PET calculation in a block.

A total of 90 blocks were drawn, each of which was assigned a unique ID. The lines defining the boundaries of the blocks were drawn using the OpenCV line command. Figure 4(a) shows the top view of the blocks which were drawn in the intersection.

Results

Time and space are important factors in critical events. Near-crash events were identified at different times of day (peak vs. off-peak hours, weekend vs. weekdays), at various stages of traffic light, and for different interaction types (car vs. car, car vs. truck, car vs. pedestrian, car vs. bicycle). Heatmaps were also created to show the parts of the intersection where near-crashes are more likely to occur. Lastly, a web-based visualization tool was developed using Grafana. This tool provides a dashboard that can be used to visualize certain outcomes of the spatio-temporal analysis. Due to the report's page constraints, enlarged versions of the graphs in this section are available in Appendix C for detailed reference.

Temporal Analysis of Near-crash Events

Average Near-crash Frequency

The frequency of near-crash events was averaged for different days of the week and times of the day, as well as weekdays versus weekends using about a month's worth of data. Figure 5(a) and 5(b) depict the analyses undertaken for weekdays and weekends to examine the interactions between cars vs. cars with a PET of less than or equal to 5 s, 4 s, 3 s, and 2 s. A comparison of these two graphs shows two different patterns for weekdays and weekends. According to Figure 5(a), on weekdays the first peak occurs between 7:00 a.m. and 8:00 a.m., aligning with the start of working hours, and it reaches its highest frequency at 4:00 p.m., which can be attributed to most workers returning from work around that time. Conversely, on weekends, as depicted in Figure 5(b), the frequency starts to increase steadily, with relatively high frequencies observed from 11 a.m. to 4 p.m. The average frequency begins to decrease from 4 p.m. on weekdays, whereas this decline starts earlier, around 2 p.m. on weekends.

Due to their lower frequencies, the most severe car-car interactions with a PET of less than or equal to 1 s are illustrated in a separate graph (see Figure 24) in Appendix D. Similar to Figures 5(a) and 5(b), one can observe a similar trend in terms of the highest frequency and peak hours. When comparing events with a PET of 1 s or less to those with a PET of 5 s or less at their highest frequency, it can be noted that the most severe interactions constitute 5% of all interactions. Any event with PET of greater than 5 s is not considered as an actual interaction.

Figures 5(c) and 5(d) present interactions between cars and trucks. On weekdays, the initial peak was observed at 7 a.m., and more or less, similar trends to car vs. car interactions were observed, albeit with significantly lower frequency. The downtrend after 4 p.m. is very sharp, suggesting that not many trucks are on the streets after this time. Also, the overall average frequency is significantly lower on weekends compared to weekdays. The interactions between cars and trucks with a PET of less than or equal to 1 s (i.e., the most severe car vs. truck interactions) are shown in Figure 25 in Appendix D. The figure shows that the frequency trend of conflicts remains relatively consistent with that of Figures 7(c and d). Similar to car vs. car interactions, the most severe car vs. truck interactions only account for 5% of all interactions.

Figures 5(e) and 5(f) depict the interactions between cars and pedestrians. The frequency steadily increases for both weekdays and weekends, and the peak frequency is observed at 4 p.m. (highest frequency slightly higher in weekdays), followed by a subsequent decrease. A morning peak frequency was not observed similar to the car vs. car and car vs. truck graphs. A similar pattern emerged for interactions with a PET of less than or equal to 1 s, albeit with a reduced frequency.

The analysis of interactions between cars and bicycles, depicted in Figures 5(g) and 5(h), shows limited interaction frequencies throughout the day, with the highest frequency recorded at seven interactions. Due to the relatively low number of interactions, discerning a specific pattern is challenging. Also, no interactions with a PET of 1 s or less were observed during both weekdays and weekends.

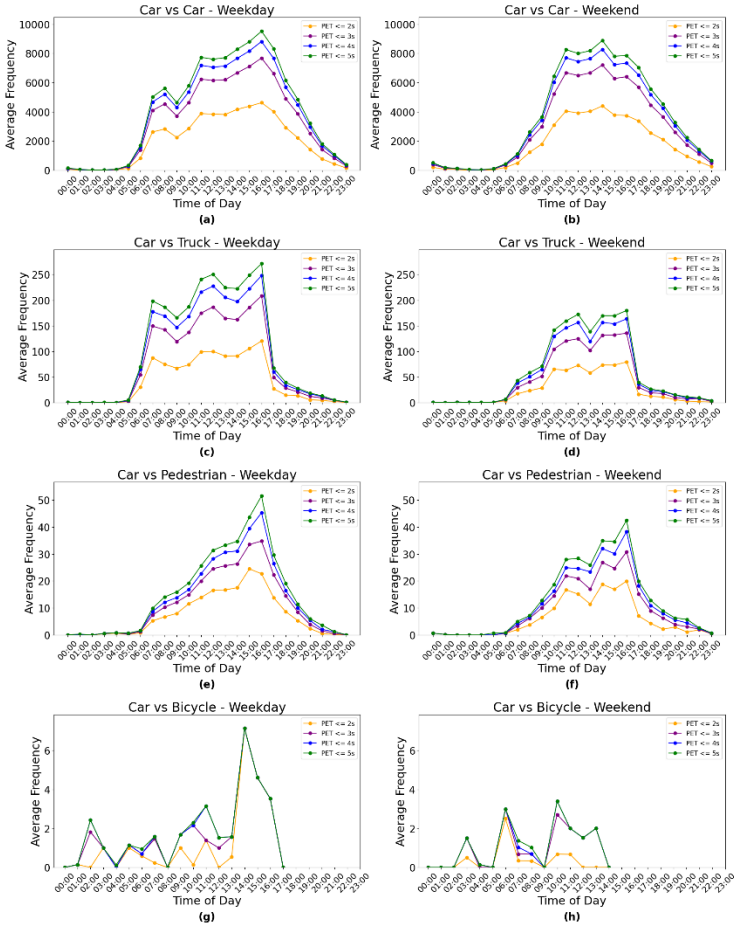

Figure 5. Graphs. Average frequency of interactions by hour during weekdays and weekend; (a, b) car vs. car, (c, d) car vs. truck, (e, f) car vs. pedestrian, and (g, h) car vs. bicycle.

An analysis of near-crashes by the day of the week for different interaction types was conducted (Figure 6). It should be noted that for visibility purposes the y-axis scaling is different for the graphs in the figures. These patterns suggest that specific weekdays may experience heightened traffic congestion and interactions among road users, contributing to an increased likelihood of near-crash events. The decrease in frequency starting from Thursday can be attributed to the approaching weekend. As shown in Figure 6, it is evident that the most frequent interactions occur between cars and cars, followed by interactions between cars and trucks. The subgraphs generally exhibit a consistent trend of fluctuating frequencies over the days of the week, except for car vs. truck interactions, which steadily decrease after Thursday and continue to decline until Sunday.

Near-crash Risk

An analysis was conducted to compare the risks of near-crash events during weekdays versus weekends at different times of the day, as well as days of the week for different interaction types. Using a generic risk formula in equation 1, risk was calculated by dividing the number of unsafe situations (i.e., frequency of near-crash events with a selected PET threshold) by the exposure events (defined as the frequency of all viable interactions; i.e., frequency of near-crashes with a PET threshold equal to or less than 5 s).

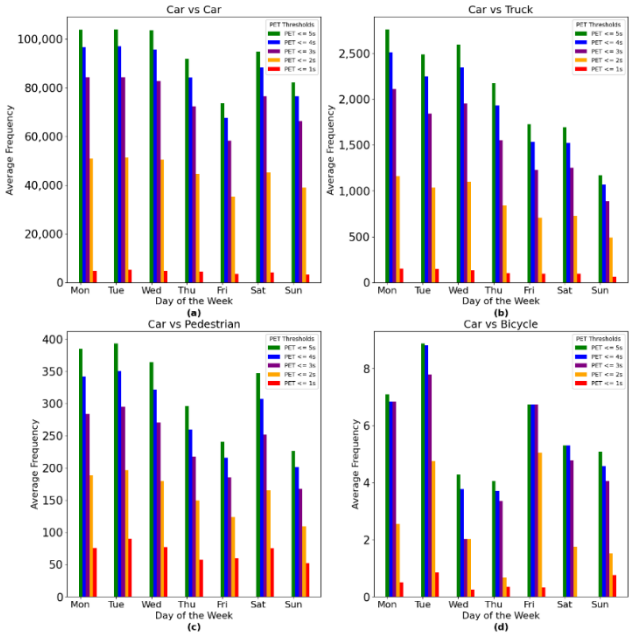

Figure 6. Graphs. Average frequency of interactions per day (a) car vs. car, (b) car vs. truck, (c) car vs. pedestrian, and (d) car vs. bicycle.

Figure 7(a) presents the risks associated with interactions between cars and cars on weekdays. Despite Figure 5(a) indicating the highest frequency of interactions during weekdays occurring at 4 p.m., the risk levels are almost constant, except for the midnight to 6 a.m. timeframe. Looking at more severe interactions (interactions with PET < 2 s), the highest risk occurs at 7 a.m., and then it gradually goes down towards the end of the day. The risk patterns for both weekdays and weekends, Figures 7(a) and 7(b), follow a similar trend. This suggests that the risk profiles associated with car vs. car interactions remain consistent regardless of whether it is a weekday or a weekend. Risk values associated with more severe interactions (i.e., with PET < 2 s) are slightly higher during weekends from midnight to 4 a.m. compared to weekdays, suggesting riskier behaviors on weekends at that time.

Risks associated with car vs. truck interactions during weekdays (Figure 7[c]) and weekends (Figure 7[d]) show similar patterns. On both weekdays and weekends, there are fluctuations and some missing data from midnight until early morning. Subsequently, risk values remain relatively constant, followed by some fluctuations towards midnight. At specific hours like 12 a.m. on weekdays or 2 a.m. on weekends, the risk for interactions with a PET of less than or equal to 4 s equals 1. There are also some zero values for risk from 2 a.m. to 4 a.m. on weekends. These outliers, as well as the missing data, are there due to either limited number of observations or the absence of trucks at certain times of the day.

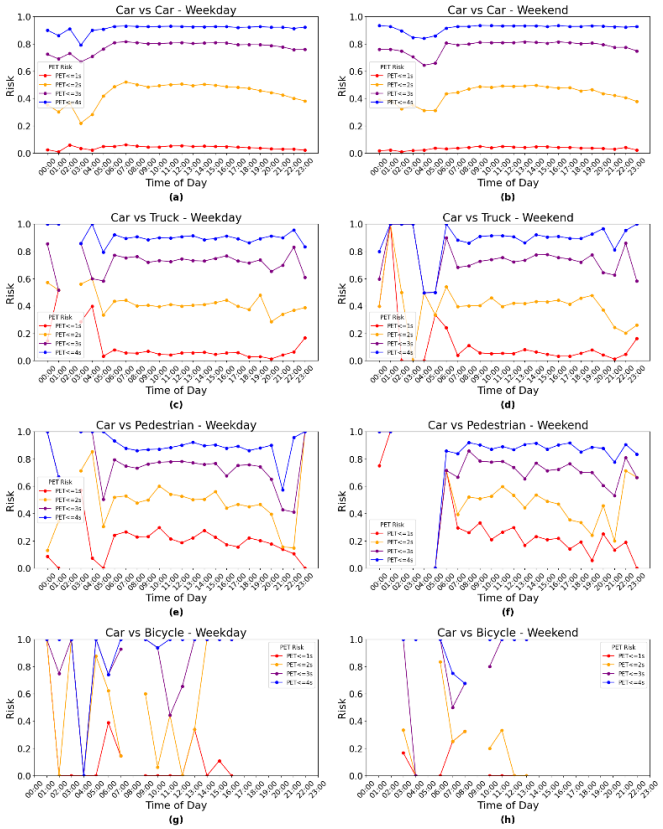

Figure 7. Graphs. Risk of near-crashes per hour during weekdays and weekend; (a, b) car vs. car, (c, d) car vs. truck, (e, f) car vs. pedestrian, and (g, h) car vs. bicycle.

Risk variations for car-pedestrian and car-bicycle interactions are illustrated in Figures 7(e and f) and Figure 7(g and h), respectively. However, insufficient car-pedestrian interactions from evenings till mornings, as well as insufficient car-bike interactions throughout the day, contribute to some fluctuations, especially for car-bike interactions, and thus no clear patterns are observed. From around 10 a.m. to 4 p.m. when car-pedestrian interaction frequency is at the highest level, risk values show a steady and almost constant trend followed by a slight decline. Similar to car-car interactions, although the car-pedestrian frequency shows an upward trend reaching its highest at around 4 p.m. (Figure 5[e] and 5[f]), the risk values are almost constant, and there is no clear peak. As shown in Figure 7, looking at more severe car-pedestrian interactions (with PET < 1 s), risk values are generally higher (~0.2) compared to car-car or car-truck interactions (~0.05).

Another risk analysis was conducted across different days of the week for various types of interactions, as shown in Figure 8. Risk values for all interaction types are steady and constant, except for car-bike interactions due to insufficient car-bike observations. Flat risk graphs show that no particular day experiences a higher risk for different interaction types, although Fridays and weekends typically have fewer interaction frequencies, as shown in Figure 6. Comparing Figure 8(a), Figure 8(b), and Figure 8(c), risk values for car-car interactions (with PET < 4 s or < 3 s or < 2 s) are slightly higher than those of car-truck and car-pedestrian interactions, suggesting that most people typically maintain a higher time headway when interacting with trucks and

pedestrians. However, similar to what Figures 7(e) and 7(f) show, and looking at more severe car-pedestrian interactions (with PET < 1 s), now with a greater number of observations (day in Figure 8 vs. hour in Figure 7), risk values are consistently higher (~0.2) compared to car-car or car-truck interactions (~0.05). This indicates that the risk of occurrence in car-pedestrian interactions, when the PET is less than 1 s, is higher compared to other types of interactions.

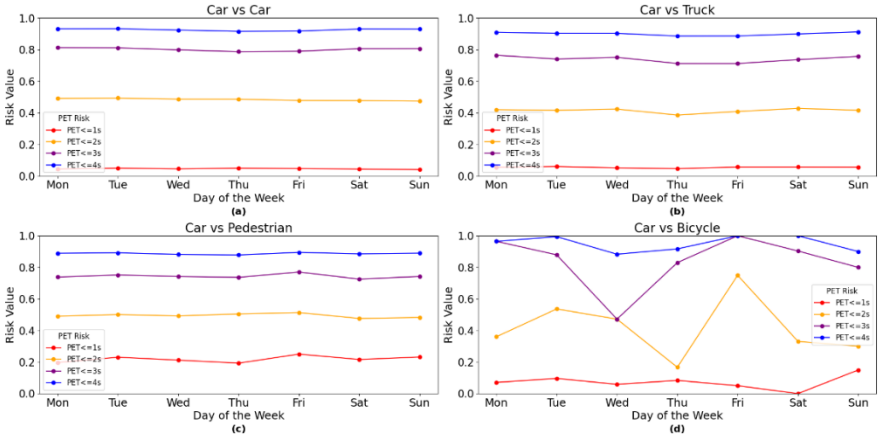

Figure 8. Graphs. Risk of near-crashes over the week for (a) car-car, (b) car-truck, (c) car-pedestrian, and (d) car-bike interactions.

Analysis of Near-crash Events During Different Stages of Signal

An analysis of near-crashes during different stages of the traffic signals was conducted for three days, specifically June 13, 14, and 15, 2023, using the camera facing H Street west. This analysis only accounts for interactions with a PET of less than 3 s, focusing on more severe interactions. Also, due to an insufficient number of observations for car-pedestrian, car-bike, and car-truck interactions, only car-car interactions are discussed.

Table 1. Car vs. Car Interactions at Various Signal Stages as a Percentage of the Total

Stage of Signal	Percentage of the Total
Red-Red	1.5%
Red-Yellow	0.81%
Red-Green	8.10%
Yellow-Yellow	0.62%
Yellow-Green	2.98%
Green-Green	85.99%

As expected, the majority of interactions involving cars vs. cars occurred when both objects were at the green stage (Table 1). This finding aligns with the higher frequency of interactions during this stage due to simultaneous movement of road users. Conversely, the lowest percentages for car vs. car interactions are observed when at least one of the objects is at the yellow stage. For instance, the red-red stage scenario means that both road objects were in the red signal stage, and the possibility of these interactions could be observed where both objects might have taken a right turn from the same street while the signal was red. Different examples of conflicts at various stages of

the traffic signal are depicted in Appendix D, Figure 26. To understand how the numbers were derived in Table 1, consider the green-green signal stage. Out of 4,333 total interactions that took place in less than 3 seconds, 3,726 of them happened when both objects were actively in the green stage. This significant proportion of interactions during the green stage is how we arrive at the 85.99% figure.

Table 2. Risk Values for Car vs. Car Interactions at Various Signal Stages

Stage of Signal	Percentage of the Total
Red-Red	75%
Red-Yellow	67%
Red-Green	74%
Yellow-Yellow	100%
Yellow-Green	75%
Green-Green	81%

Another analysis was conducted to evaluate the risk of events during different stages of the signal. Risk values were obtained by dividing the frequency of events with a PET of less than 3 s by the frequency of events with PET of less than 5 s within each traffic signal stage combination (e.g., Red vs. Red). Table 2 demonstrates that the risk values for car vs. car interactions is the highest when both cars are in the yellow stage. This observation appears reasonable, as drivers aim to clear the intersection before facing the red light, resulting in more aggressive behavior during these stages compared to others. The second highest risk values are observed when both cars are in the green stage. To elucidate the calculations behind Table 2, the procedure involved dividing the count of interactions with a PET of 3 seconds or less by the total count of interactions with a PET of 5 seconds or less, all within the same signal stage. Taking the yellow-yellow stage as an example, the risk value is displayed as 100%. This signifies that every interaction occurring while both objects were in the yellow stage of the signal resulted in a PET of 3 seconds or less. Specifically, there were 27 such interactions. Coincidentally, the total count of interactions with a PET of 5 seconds or less was also 27. This leads to the calculated risk percentage of 100%.

Edge Computation

Video from each Hikvision camera was transmitted using RTSP at a pixel resolution of 1280 × 720 (e.g., 720p or standard high definition) and a frame rate of 10 frames/second. With Motion JPEG compression (MJPG-10), an estimated data rate of 11.4 Mb/s was required to stream each video to SDSU for processing and archival. With four cameras streaming simultaneously, 45.7 Mbps was required. Verizon 4G LTE wireless broadband supports typical upload speeds of 5 Mbps, with a theoretical maximum peak upload data-rate of 50 Mbps. Packet loss occurring over a 4G LTE network results in frame loss, which amounted to 4%, leading to the loss of nearly 1,440 frames out of 36,000 frames in a 1-hour video. With four cameras streaming at only 10 frames/second, which is not real-time (e.g., 30 frames/second), the required data rate of 45.7 Mbps was near the maximum peak upload data rate of 50 Mbps. From the limited supported data rate, we see that streaming intersection video to a central source over a single cellular 4G LTE link is

not scalable beyond more than one intersection per LTE transceiver/modem. A scalable scheme is to stream each camera video to a local device capable of performing vehicle object detection and tracking, so video processing can be performed locally rather than centrally. In the traffic signal control cabinet, we installed four Nvidia Jetson AGX Xavier edge computing devices, one assigned to each camera. These Jetsons were connected to a switched 100 Mbps Local Area Ethernet Network that also connects to the four Hikvision cameras. With 100 Mbps > 45.7 Mbps, the probability of frame loss is substantially reduced. Each camera streams video to an assigned Jetson, where object detection and tracking is performed. In this edge-based scheme, only the results of object detection and tracking are transmitted back to SDSU over the 4G LTE network. Results consist of a database record with a timestamp indicating the event where a detected vehicle crosses a grid line boundary along with five, four-byte integers and a mode string that specifies a vehicle classification label (e.g., car, truck, van). Typical record lengths are 30 bytes; at a typical upload rate of 5 Mbps, a typical vehicle event record can be transmitted from a Jetson to SDSU over 4G LTE in 48 μs, making an edge-based object detection and tracking scheme scalable to accommodate data capture from multiple intersections over a single 4G LTE link.

Web-based Tool Development

A web-based tool was developed that can be used by practitioners to visualize data and perform safety evaluations. The tool offers various analyses, such as traffic volume for different road users, daily traffic patterns, movement types, near-crash events, PET by interaction type, risk calculations, and the temporal and spatial distribution of critical conflicts. The tool was developed with Grafana, which is an open-source data visualization and analytics platform. It is a suitable platform for visualizing complex data sets and metrics, providing a user-friendly web interface with drag-and-drop features to create customized dashboards that can be shared across teams and organizations. Grafana supports a wide range of data sources, including databases, cloud services, and third-party applications. A MySQL database was developed to store the data and was linked to Grafana for creating interactive dashboards and charts. The combination of MySQL and Grafana provided an effective solution for collecting, storing, and visualizing data. Grafana, version 8.5.22, was used in conjunction with the ImageIt plugin, version 1.0.7. The dashboard retrieved data from the MySQL tables created using phpMyAdmin.

The dashboard consists of two main sections: Volume and PET Interactions. Each section includes various analyses, referred to as panels, all of which are outlined in detail in Table 3 found in Appendix E. Figure 10 provides an overview of the dashboard presented in a video wall located in the Smart Transportation Analytics Research (STAR) lab at SDSU.

Dashboard variables were defined to enable data filtering and query computations. These variables were utilized in specific panels, providing users with the ability to customize and tailor their data analysis. Table 3 and 4 in Appendix E outline the variables within the dashboard.

Spatial safety assessment results are visualized using two panels (Figure 11) powered by the ImageIt Grafana plug-in, facilitating a spatial visualization of interaction severity frequency (part a) and risk (part b) within a designated block area and intersection across defined time intervals.

Figure 9. Screen capture. Dashboard overview.

In the "Intersection PET Heatmap" panel, the more dangerous the interaction in terms of the PET threshold, the higher its weight; if there is no interaction, a count value of zero is assigned. Colors were assigned to each block for Figure 11(a) based on the combined frequency of verydangerousPET, dangerousPET, and mildPET interactions using the following thresholds: green for frequencies below 50, yellow for frequencies between 50 and 100, orange for frequencies between 100 and 200, and red for frequencies greater than 200.

In the "Normalized Heatmap" panel, risk calculations for each block are determined using Equation 1, where interactions with a PET of less than 2 s are considered unsafe situations, while interactions with a PET of less than 5 s represent exposure situations. These thresholds are user configurable within the dashboard. In Figure 11(b), a similar threshold-based approach is adopted to visualize risk. Colors are assigned based on risk values, with green indicating risk values below 5%, yellow 5% to 10%, orange 10% to 20%, and red exceeding 20%.

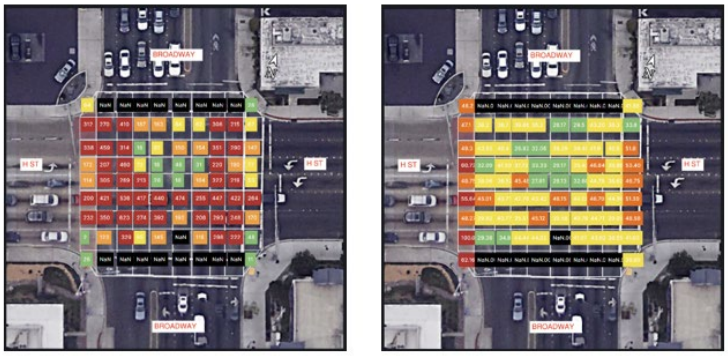

(a) (b)

Figure 10. Screen capture. Interaction PET heatmap panel: (a) frequency, (b) risk.

The descriptions of other dashboard panels can be found in Appendix E for reference.

Conclusions

This study developed an ITMC focusing on proactive intersection safety assessment. Near-crash event identification using PET as an SSM was utilized to identify potentially risky situations. At a signalized intersection in Chula Vista, video data were used to deploy deep learning models to detect and classify moving objects within the video frames. Model deployment was conducted both on a central server and on edge computation devices. For model development, YOLOX was used as the deep learning modeling framework. The outcomes of the computer vision models were used to compute PET values for various interaction types.

The temporal analysis showed that car versus car interactions dominated, with the lowest interaction frequency involving cars and bicycles, reflecting the limited presence of bicycles at the intersection. Interaction frequency was lower on weekends compared to weekdays. Weekdays exhibited two peaks for car-car and car-truck interactions, coinciding with the start and end of the workday, at 8 a.m. and 4 p.m. On weekends, a single peak occurred for car-car and car-pedestrian interactions at 2 p.m. and 4 p.m., respectively. Looking at daily charts, average interaction frequency shows a reduction towards the end of the week, particularly on Thursday and Friday, with a slight uptick on Saturdays. Despite variations in event frequencies across different times of day and days of the week, risk values displayed a consistent trend throughout both weekdays and weekends, remaining relatively stable across different days and across the majority of the day.

An edge-based computation approach was compared against a cloud-based computation approach, highlighting the scalability issue of centralized systems, as well as transmission data loss issues. A single cellular 4G LTE link at its peak data rate is only capable of handling one intersection with four cameras each streaming a standard high-definition footage at 10 frames per second. An edge-based object detection and tracking scheme is scalable to accommodate data capture from multiple intersections over a single 4G LTE link. This way, video processing is performed locally, and only the results of object detection and tracking are transmitted back to a central location, which is significantly smaller in size compared to the amount of data that needs to be transferred in a cloud-based system.

In the analysis of interactions at different signal stages, the majority occurred when the signal was green for both objects involved, with the highest risk observed during the yellow stage for both objects. This finding aligns with the perception that drivers may be more inclined to rush through the intersection during the yellow phase, resulting in riskier interactions.

Lastly, a web dashboard was developed using Grafana that can serve as a platform for assessing safety and visualizing the outcomes for an intersection.

Additional Products

The outcomes of the Education and Workforce Development and Technology Transfer from this project can be found on the project page of the Safe-D website.

Education and Workforce Development Products

The following Education and Workforce Development items resulted from project activities:

1. A total of seven students (one CCEE grad student, five ECE grad students, and one CCEE undergraduate student) took part in this project.
    a. One CCEE Master's student, Sina Salehipour, was engaged in all the activities of the project. The student automated the computation of PET for the intersection in Chula Vista and created a dashboard for visualizing the results. The project has been incorporated into the student's master's thesis. Additionally, the student is presently working on a research paper, and it is anticipated that the student will defend their MS thesis in the Fall of 2023.
    b. ECE Master's project student Naga Dheeraj Kurapati investigated methods for segmenting images from camera intersection videos to identify the road region from non-road regions and dynamically overlay a grid on the road region to compute PET.
    c. ECE Master's thesis student Erfan Chowdhury Shourov investigated deep learning architectures for skateboarder-pedestrian SSMs. Shourov captured a large image dataset of pedestrians and skateboarders on the campus of SDSU and used this image dataset to train the Faster R-CNN model and the SSD model to detect and classify pedestrians and skateboarders. The positions of pedestrians and skateboarders were then used to measure PET and TTC SSMs. This effort led to the publication of one journal article, one conference paper, and two image datasets.
    d. ECE Master's project student Ugur Emre Dogan investigated real-time object tracking models that were executed on the NVIDIA Jetson AGX Xavier using the DeepStream SDKs and NVIDIA JetPack, OpenCV, cuDNN, CUDA®, and the TensorRT C++/Python libraries. Dogan implemented and trained an object detection and classification model, with re-identification, to recognize vehicles, pedestrians, mopeds, bicycles, scooters, and motorcycles.
    e. ECE Master's project student Arya Yazdani investigated the quantization of the trained Faster R-CNN and SSD models developed by Shourov for deployment on Coral EdgeTPU boards. Yazdani *froze* (i.e., saved weights and bias values) the models trained by Shourov, quantized the frozen models, converted the quantized models into TensorFlow TFLite models, and deployed the models on a Coral EdgeTPU board.
    f. Computer Science student Rishita Bapu Mote investigated optical character recognition algorithms and implemented methods to decipher the overlayed video timestamp added by Hikvision cameras.

g. CCEE undergrad student, Django Bergcollins, assisted in the SQL database system development and the web-based visualization tool development.

2. The project outcomes were used in a course offered in the ECE department, Computer Engineering 596. The slides show how a topic discussed in this course, accelerated discrete convolution, is relevant to the ITMC.

3. The project contributed to a graduate course on ITS offered in the CCEE department (CIVE 696 Intelligent Transportation Systems).

4. Salehipour, S., A. Jahangiri, C. Paolini, and S. Ghanipoor Machiani. Monitoring Road Users' Interactions at a Signalized Intersection with a Surrogate Safety Measure (PET): A Deep-learning-based (YOLOX) Computer Vision Approach. 2022 Student Research Symposium, San Diego State University.

Technology Transfer Products

The following technology transfer products resulted from project activities:

- The ITMC testbed was developed as described in detail in this report. The testbed can be used in the future by the city, researchers, and students to conduct research and test different technology.

- The team met with the City of Chula Vista several times over the course of the project to build the testbed, as well as to obtain feedback on how the ITMC could help the city with safety assessments.

- A web-based tool was developed to visualize some of the project outcomes. The tool can be used to perform temporal and special safety analyses and to identify when and where near-crash situations occur the most.

- Shourov, E. C., M. Sarkar, A. Jahangiri, and C. Paolini, C. Deep Learning Architectures for Skateboarder–Pedestrian Surrogate Safety Measures. *Future Transportation*, Vol. 1, 2021, No. 2, pp, 387-413.

- E. C. Shourov and C. Paolini. Laying the Groundwork for Automated Computation of Surrogate Safety Measures (SSM) for Skateboarders and Pedestrians using Artificial Intelligence. 2020 Third International Conference on Artificial Intelligence for Industries (AI4I), Irvine, CA, USA, 2020, pp. 19-22, doi: 10.1109/AI4I49448.2020.00011.
- E. C. Shourov and C. Paolini. Skateboarder and Pedestrian Conflict Zone Detection Dataset. November 14, 2020. Available: osf.io/nyhf7, doi: 10.17605/OSF.IO/NYHF7.
    - http://dx.doi.org/10.17605/OSF.IO/NYHF7
- C. Paolini, C. E. Shourov, A. Jahangiri, and S. G. Machiani. Skateboarder and Pedestrian Dataset. January 30, 2020. [Online]. Available: osf.io/cqd9z, doi: 10.17605/OSF.IO/CQD9Z.
    - http://dx.doi.org/10.17605/OSF.IO/CQD9Z

- Salehipour, S., A. Jahangiri, C. Paolini, and S. Ghanipoor Machiani. Monitoring Road Users' Interactions at a Signalized Intersection with a Surrogate Safety Measure (PET): A Deep-learning-based (YOLOX) Computer Vision Approach. 2022 NSF AI in Transportation Workshop, Hilton University of Florida Conference Center in Gainesville, Florida.

- The team is currently working on a journal paper.

Data Products

- Link to Datasets: https://doi.org/10.15787/VTT1/P9GYI6 *
- Project Description – The goal of this project was to develop an intelligent transportation management center (ITMC) with a focus on proactive safety assessment.
- Data Scope – One month of road user interaction data at a signalized intersection in the City of Chula Vista, captured by four cameras installed on signal mast arms within the intersection. This resulted in a dataset comprising 3.8 million rows. Each row has a potential interaction between road users, depending on the variables observed.
- Data Specification – A detailed description of each variable in the dataset can be found in Appendix F.
- Citation Metadata:
    - Title of datasets: "SafeD-ChulaVista-04-110-Data.csv"
    - Author list with researcher ORCIDs
        - Arash Jahangiri, 0000-0002-8825-961X
        - Chris Paolini, 0000-0001-6563-917X
        - Sina Salehipour, 0009-0006-5275-6784
        - Django Bergcollins, 0009-0006-2591-0184
    - Contact information (email) for corresponding author: AJahangiri@sdsu.edu

Keywords: Intelligent Transportation Management Center (ITMC), Proactive safety evaluation, Surrogate safety measures (SSM), Smart Cities, YOLOX, Post encroachment time (PET)

References

1. Kimley-Horn and Associates, Inc. Traffic Management Centers in a Connected Vehicle Environment. https://docplayer.net/2946497-Traffic-management-centers-in-a-connected-vehicle-environment.html. Accessed Sep. 4, 2023.

2. Stevanovic, A., J. Stevanovic, and C. Kergaye. Optimization of Traffic Signal Timings Based on Surrogate Measures of Safety. *Transportation Research Part C: Emerging Technologies*, Vol. 32, 2013, pp. 159–178. https://doi.org/10.1016/j.trc.2013.02.009.

3. Zohdy, I. H., and H. A. Rakha. Intersection Management via Vehicle Connectivity: The Intersection Cooperative Adaptive Cruise Control System Concept. *Journal of Intelligent Transportation Systems*, Vol. 20, No. 1, 2016, pp. 17–32. https://doi.org/10.1080/15472450.2014.889918.

4. Intersection Safety | FHWA. https://highways.dot.gov/research/research-programs/safety/intersection-safety. Accessed Sep. 5, 2023.

5. Tarko, A. P. Surrogate Measures of Safety. In *Safe Mobility: Challenges, Methodology and Solutions* (D. Lord and S. Washington, eds.), Emerald Publishing Limited, pp. 383–405.

6. Elvik, R. The Non-Linearity of Risk and the Promotion of Environmentally Sustainable Transport. *Accident Analysis & Prevention*, Vol. 41, No. 4, 2009, pp. 849–855. https://doi.org/10.1016/j.aap.2009.04.009.

7. Blincoe, L., T. R. Miller, E. Zaloshnja, and B. A. Lawrence. The Economic and Societal Impact of Motor Vehicle Crashes, 2010 (Revised). 2015.

8. Zhao, P., and C. Lee. Assessing Rear-End Collision Risk of Cars and Heavy Vehicles on Freeways Using a Surrogate Safety Measure. *Accident Analysis & Prevention*, Vol. 113, 2018, pp. 149–158. https://doi.org/10.1016/j.aap.2018.01.033.

9. Shekhar Babu, S., and P. Vedagiri. Proactive Safety Evaluation of a Multilane Unsignalized Intersection Using Surrogate Measures. *Transportation Letters*, Vol. 10, No. 2, 2018, pp. 104–112. https://doi.org/10.1080/19427867.2016.1230172.

10. Stipancic, J., L. Miranda-Moreno, and N. Saunier. Vehicle Manoeuvers as Surrogate Safety Measures: Extracting Data from the Gps-Enabled Smartphones of Regular Drivers. *Accident Analysis & Prevention*, Vol. 115, 2018, pp. 160–169. https://doi.org/10.1016/j.aap.2018.03.005.

11. Johnsson, C., A. Laureshyn, and T. De Ceunynck. In Search of Surrogate Safety Indicators for Vulnerable Road Users: A Review of Surrogate Safety Indicators. *Transport Reviews*, Vol. 38, No. 6, 2018, pp. 765–785. https://doi.org/10.1080/01441647.2018.1442888.

12. Forbes, T. W. Analysis of "near Accident" Reports. *Highway Research Board bulletin*, Vol. 152, 1957, pp. 23–37.

13. Lorion, A. C., and B. Persaud. Investigation of Surrogate Measures for Safety Assessment of Urban Two-Way Stop Controlled Intersections. *Canadian Journal of Civil Engineering*, Vol. 42, No. 12, 2015, pp. 987–992. https://doi.org/10.1139/cjce-2015-0023.

14. Wu, K.-F., and P. P. Jovanis. Screening Naturalistic Driving Study Data for Safety-Critical Events. *Transportation Research Record*, Vol. 2386, No. 1, 2013, pp. 137–146. https://doi.org/10.3141/2386-16.

15. Quispe, H., J. Sumire, P. Condori, E. Alvarez, and H. Vera. I See You: A Vehicle-Pedestrian Interaction Dataset from Traffic Surveillance Cameras. http://arxiv.org/abs/2211.09342. Accessed Sep. 4, 2023.

16. De Angelis, M., F. Fraboni, V. M. Puchades, G. Prati, and L. Pietrantoni. Use of Smartphone and Crash Risk among Cyclists. *Journal of Transportation Safety & Security*, Vol. 12, No. 1, 2020, pp. 178–193. https://doi.org/10.1080/19439962.2019.1591559.

17. Bhattarai, N., Y. Zhang, H. Liu, Y. Pakzad, and H. Xu. Proactive Safety Analysis Using Roadside LiDAR Based Vehicle Trajectory Data: A Study of Rear-End Crashes. *Transportation Research Record*, 2023, p. 03611981231182704. https://doi.org/10.1177/03611981231182704.

18. Wang, C., Y. Xie, H. Huang, and P. Liu. A Review of Surrogate Safety Measures and Their Applications in Connected and Automated Vehicles Safety Modeling. *Accident Analysis & Prevention*, Vol. 157, 2021, p. 106157. https://doi.org/10.1016/j.aap.2021.106157.

19. Wu, J., H. Xu, Y. Zheng, and Z. Tian. A Novel Method of Vehicle-Pedestrian near-Crash Identification with Roadside LiDAR Data. *Accident Analysis & Prevention*, Vol. 121, 2018, pp. 238–249. https://doi.org/10.1016/j.aap.2018.09.001.

20. Smith, D. L., W. G. Najm, and R. A. Glassco. Feasibility of Driver Judgment as Basis for a Crash Avoidance Database. *Transportation Research Record*, Vol. 1784, No. 1, 2002, pp. 9–16. https://doi.org/10.3141/1784-02.

21. Mohamed, M. G., and N. Saunier. The Impact of Motion Prediction Methods on Surrogate Safety Analysis: A Case Study of Left-Turn and Opposite-Direction Interactions at a Signalized Intersection in Montreal. *Journal of Transportation Safety & Security*, Vol. 10, No. 4, 2018, pp. 265–287. https://doi.org/10.1080/19439962.2016.1255690.

22. Perkins, S. R., and J. I. Harris. TRAFFIC CONFLICT CHARACTERISTICS: FREEWAY CURVE AND EXIT AREA F1, DECEMBER, 1966. 1967.

23. Minderhoud, M. M., and P. H. L. Bovy. Extended Time-to-Collision Measures for Road Traffic Safety Assessment. *Accident Analysis & Prevention*, Vol. 33, No. 1, 2001, pp. 89–97. https://doi.org/10.1016/S0001-4575(00)00019-1.

24. Laureshyn, A., Å. Svensson, and C. Hydén. Evaluation of Traffic Safety, Based on Micro-Level Behavioural Data: Theoretical Framework and First Implementation. *Accident Analysis & Prevention*, Vol. 42, No. 6, 2010, pp. 1637–1646. https://doi.org/10.1016/j.aap.2010.03.021.

25. Cunto, F. J. C. Assessing Safety Performance of Transportation Systems Using Microscopic Simulation.

26. Oh, C., S. Park, and S. G. Ritchie. A Method for Identifying Rear-End Collision Risks Using Inductive Loop Detectors. *Accident Analysis & Prevention*, Vol. 38, No. 2, 2006, pp. 295–301. https://doi.org/10.1016/j.aap.2005.09.009.

27. Uno, N., Y. Iida, S. Itsubo, and S. Yasuhara. A MICROSCOPIC ANALYSIS OF TRAFFIC CONFLICT CAUSED BY LANE-CHANGING VEHICLE AT WEAVING SECTION.

28. Rahman, M. S., M. Abdel-Aty, L. Wang, and J. Lee. Understanding the Highway Safety Benefits of Different Approaches of Connected Vehicles in Reduced Visibility Conditions. *Transportation Research Record*, Vol. 2672, No. 19, 2018, pp. 91–101. https://doi.org/10.1177/0361198118776113.

29. Astarita, V., G. Guido, and A. Vitale. A New Microsimulation Model for the Evaluation of Traffic Safety Performances. No. 51, 2012.

30. Okamura, M., A. Corporation, A. Fukuda, H. Morita, H. Suzuki, and M. Nakazawa. IMPACT EVALUATION OF A DRIVING SUPPORT SYSTEM ON TRAFFIC FLOW BY MICROSCOPIC TRAFFIC SIMULATION.

31. Barceló, J., A.-G. Dumont, L. Montero, J. Perarnau, and A. Torday. SAFETY INDICATORS FOR MICROSIMULATION- BASED ASSESSMENTS. 2003.

32. Shelby, S. G. DELTA-V AS A MEASURE OF TRAFFIC CONFLICT SEVERITY.

33. Bagdadi, O. Estimation of the Severity of Safety Critical Events. *Accident Analysis & Prevention*, Vol. 50, 2013, pp. 167–174. https://doi.org/10.1016/j.aap.2012.04.007.

34. Laureshyn, A., T. De Ceunynck, C. Karlsson, Å. Svensson, and S. Daniels. In Search of the Severity Dimension of Traffic Events: Extended Delta-V as a Traffic Conflict Indicator. *Accident Analysis & Prevention*, Vol. 98, 2017, pp. 46–56. https://doi.org/10.1016/j.aap.2016.09.026.

35. Ozbay, K., H. Yang, B. Bartin, and S. Mudigonda. Derivation and Validation of New Simulation-Based Surrogate Safety Measure. *Transportation Research Record*, Vol. 2083, No. 1, 2008, pp. 105–113. https://doi.org/10.3141/2083-12.

36. Alhajyaseen, W. K. M. The Integration of Conflict Probability and Severity for the Safety Assessment of Intersections. *Arabian Journal for Science and Engineering*, Vol. 40, No. 2, 2015, pp. 421–430. https://doi.org/10.1007/s13369-014-1553-1.

37. Akhavian, R., A. Jahangiri, F. Shahnavaz, and S. Salehipour. *A Holistic Work Zone Safety Alert System through Automated Video and Smartphone Sensor Data Analysis*. Safe-D National UTC, 2022.

38. Redmon, J., S. Divvala, R. Girshick, and A. Farhadi. You Only Look Once: Unified, Real-Time Object Detection. Presented at the 2016 IEEE Conference on Computer Vision and Pattern Recognition (CVPR), 2016.

39. Ren, S., K. He, R. Girshick, and J. Sun. Faster R-CNN: Towards Real-Time Object Detection with Region Proposal Networks. http://arxiv.org/abs/1506.01497. Accessed Sep. 5, 2023.

40. Liu, W., D. Anguelov, D. Erhan, C. Szegedy, S. Reed, C.-Y. Fu, and A. C. Berg. SSD: Single Shot MultiBox Detector, pp. 21–37.

41. Shourov, C. E., M. Sarkar, A. Jahangiri, and C. Paolini. Deep Learning Architectures for Skateboarder–Pedestrian Surrogate Safety Measures. *Future Transportation*, Vol. 1, No. 2, 2021, pp. 387–413. https://doi.org/10.3390/futuretransp1020022.

42. Ge, Z., S. Liu, F. Wang, Z. Li, and J. Sun. YOLOX: Exceeding YOLO Series in 2021. http://arxiv.org/abs/2107.08430. Accessed Sep. 5, 2023.

43. Zangenehpour, S., J. Strauss, L. F. Miranda-Moreno, and N. Saunier. Are Signalized Intersections with Cycle Tracks Safer? A Case–Control Study Based on Automated Surrogate Safety Analysis Using Video Data. *Accident Analysis & Prevention*, Vol. 86, 2016, pp. 161–172. https://doi.org/10.1016/j.aap.2015.10.025.

44. Kumar, A., M. Paul, and I. Ghosh. Analysis of Pedestrian Conflict with Right-Turning Vehicles at Signalized Intersections in India. *Journal of Transportation Engineering, Part A: Systems*, Vol. 145, No. 6, 2019, p. 04019018. https://doi.org/10.1061/JTEPBS.0000239.

45. Marisamynathan, S., and P. Vedagiri. Pedestrian Safety Evaluation of Signalized Intersections Using Surrogate Safety Measures. *Transport*, Vol. 35, No. 1, 2020, pp. 48–56. https://doi.org/10.3846/transport.2020.12157.

46. Peesapati, L. N., M. P. Hunter, and M. O. Rodgers. Evaluation of Postencroachment Time as Surrogate for Opposing Left-Turn Crashes. *Transportation Research Record*, Vol. 2386, No. 1, 2013, pp. 42–51. https://doi.org/10.3141/2386-06.

Appendices

Appendix A

The *notos.sdsu.edu* server is specifically designed to store and process large amounts of data. *notos.sdsu.edu* is a Supermicro SuperServer 4028GR-TR GPU cluster optimized for AI, deep learning, and/or HPC applications. *notos.sdsu.edu* features 8x NVIDIA® Tesla V100-PCIe GPUs and has the TensorFlow, TensorFlow Lite, Caffe, PyTorch, and Keras deep learning frameworks installed. In addition, *notos.sdsu.edu* is connected to the SDSU *Beehive* BeeGFS petascale network-accessible storage system capable of parallel I/O for use in high-performance computing numerical simulations and data acquisition processes. The BeeGFS storage cluster has a capacity of 2.4 PB and consists of two metadata servers (SuperMicro SuperStorage Server 2028R-E1CR24H) and four object storage servers (QCT 4U 78 Bays High Density Storage Server 1S2PZZZ0007) and contains a total of 4 x 78 x 8 TB HDDs. The storage cluster supports MPI-IO, parallel NetCDF, and parallel HDF5 to improve run-time performance of I/O bound computations.

To deal with the large data size, ITMC is currently developing disruptive technologies that perform machine learning in situ to detect road users in real-time. Known as *inferencing at the edge*, these technologies allow one to perform computationally intensive AI calculations locally at the intersection on a Jetson device without needing to transfer streaming video to a graphics processing unit (GPU) server (such as *notos.sdsu.edu*) at a centralized facility to perform calculations. These Jetsons will perform continuous, real-time image classification of vehicles and pedestrians that enter the camera field of view, using a mobile GPU to execute accelerated convolutional neural network (CNN) deep-learning models trained using the PyTorch framework with live image data streamed to each Jetson from each Hikvision camera. These CNN deep-learning models are capable of real-time recognition of road users and can implement in situ near-crash identification capabilities that can be utilized in proactive risk calculation and potentially can be integrated into traffic controller systems for crash prevention and mitigation.

Appendix B

An example of stored data in phpMyAdmin is shown below:

ObjectID	BlockID	Mode	LineID	Time ▼ 1	FarameNo	Camera
1928	24	car	36	2023-04-02 00:00:00	35995	8005
1928	25	car	36	2023-04-02 00:00:00	35995	8005
1928	25	car	38	2023-04-02 00:00:00	35997	8005
1936	21	car	28	2023-04-01 23:59:59	35987	8005
1939	80	car	84	2023-04-01 23:59:59	35987	8005
1939	80	car	84	2023-04-01 23:59:59	35988	8005
1936	21	car	30	2023-04-01 23:59:59	35989	8005
1936	22	car	30	2023-04-01 23:59:59	35989	8005
1936	22	car	32	2023-04-01 23:59:59	35992	8005
1936	23	car	32	2023-04-01 23:59:59	35992	8005
1936	23	car	34	2023-04-01 23:59:59	35994	8005
1936	24	car	34	2023-04-01 23:59:59	35994	8005
1939	80	car	84	2023-04-01 23:59:58	35983	8005
1939	80	car	84	2023-04-01 23:59:58	35984	8005
1928	23	car	34	2023-04-01 23:59:53	35929	8005
1928	24	car	34	2023-04-01 23:59:53	35929	8005
1928	24	car	36	2023-04-01 23:59:53	35931	8005
1928	25	car	36	2023-04-01 23:59:53	35931	8005
1928	25	car	38	2023-04-01 23:59:53	35932	8005
1934	61	car	72	2023-04-01 23:59:47	35870	8005
1934	61	car	72	2023-04-01 23:59:47	35871	8005
1934	80	car	84	2023-04-01 23:59:46	35858	8005
1928	23	car	34	2023-04-01 23:59:39	35787	8005
1928	24	car	34	2023-04-01 23:59:39	35787	8005
1928	24	car	36	2023-04-01 23:59:39	35789	8005
1928	25	car	36	2023-04-01 23:59:39	35789	8005
1928	25	car	38	2023-04-01 23:59:39	35790	8005
1928	21	car	28	2023-04-01 23:59:38	35779	8005
1928	21	car	30	2023-04-01 23:59:38	35781	8005
1928	22	car	30	2023-04-01 23:59:38	35781	8005
1928	21	car	30	2023-04-01 23:59:38	35782	8005
1928	22	car	30	2023-04-01 23:59:38	35782	8005
1928	22	car	32	2023-04-01 23:59:38	35784	8005
1928	23	car	32	2023-04-01 23:59:38	35784	8005
1924	2	car	6	2023-04-01 23:59:26	35655	8005
1924	3	car	6	2023-04-01 23:59:26	35655	8005
1924	2	car	6	2023-04-01 23:59:26	35656	8005
1924	3	car	6	2023-04-01 23:59:26	35656	8005
1924	2	car	7	2023-04-01 23:59:26	35657	8005
1924	14	car	24	2023-04-01 23:59:25	35647	8005
1924	24	car	24	2023-04-01 23:59:25	35647	8005
1924	13	car	23	2023-04-01 23:59:25	35648	8005
1924	14	car	23	2023-04-01 23:59:25	35648	8005
1924	3	car	8	2023-04-01 23:59:25	35653	8005
1924	13	car	8	2023-04-01 23:59:25	35653	8005

Appendix C

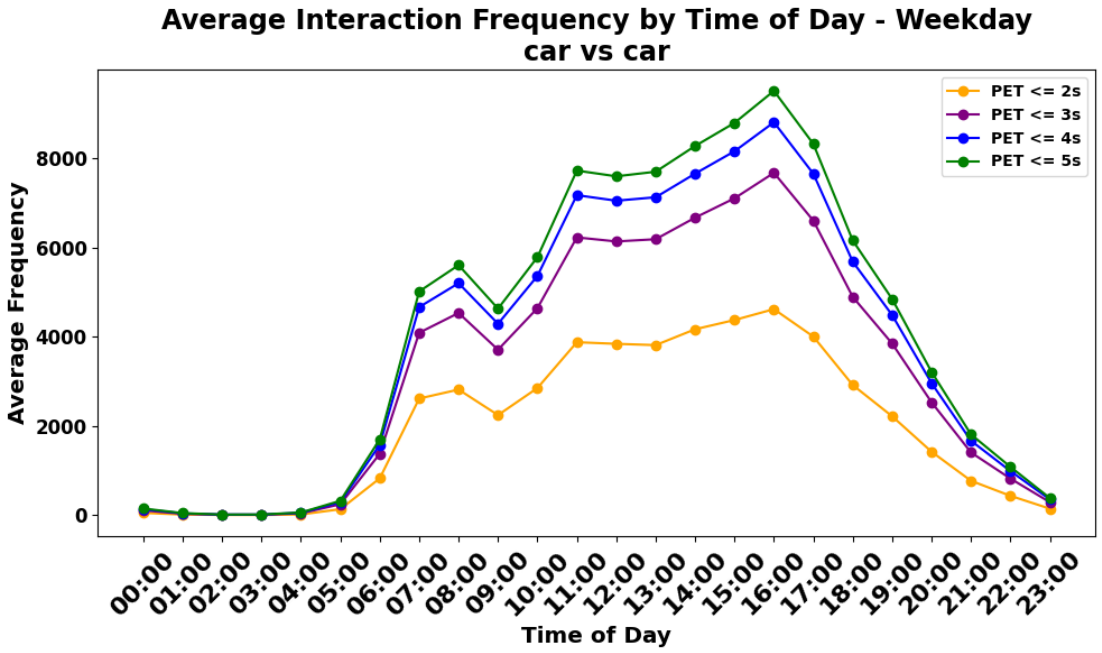

(a)

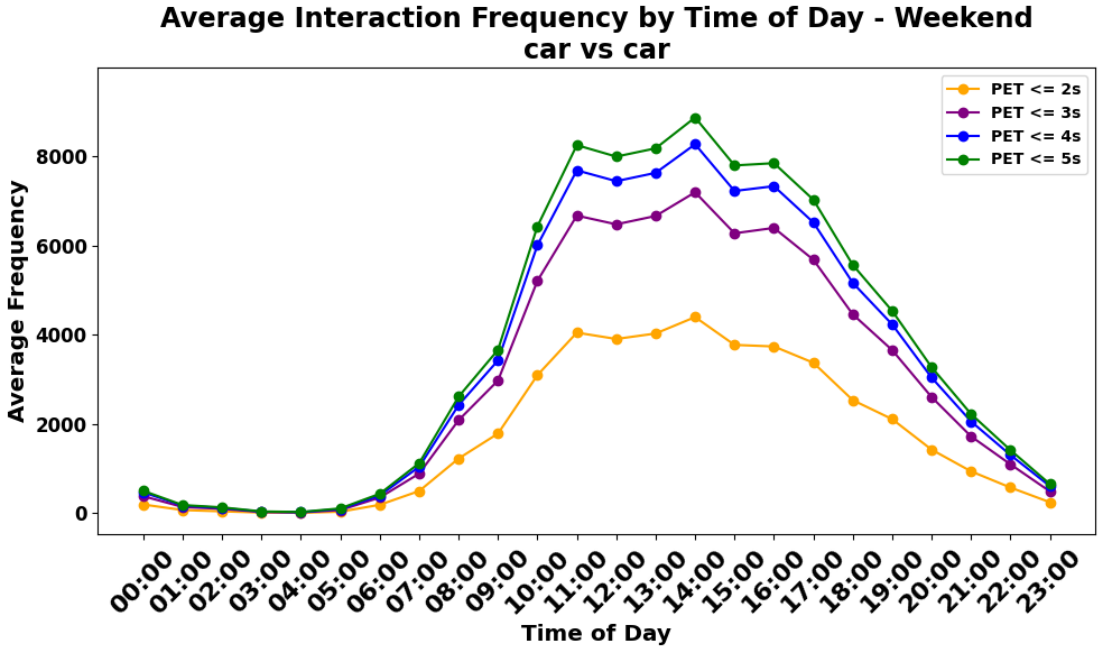

(b)

Figure 11. Graph. Average frequency of car vs. car interactions by hour; (a) weekdays, (b) weekends.

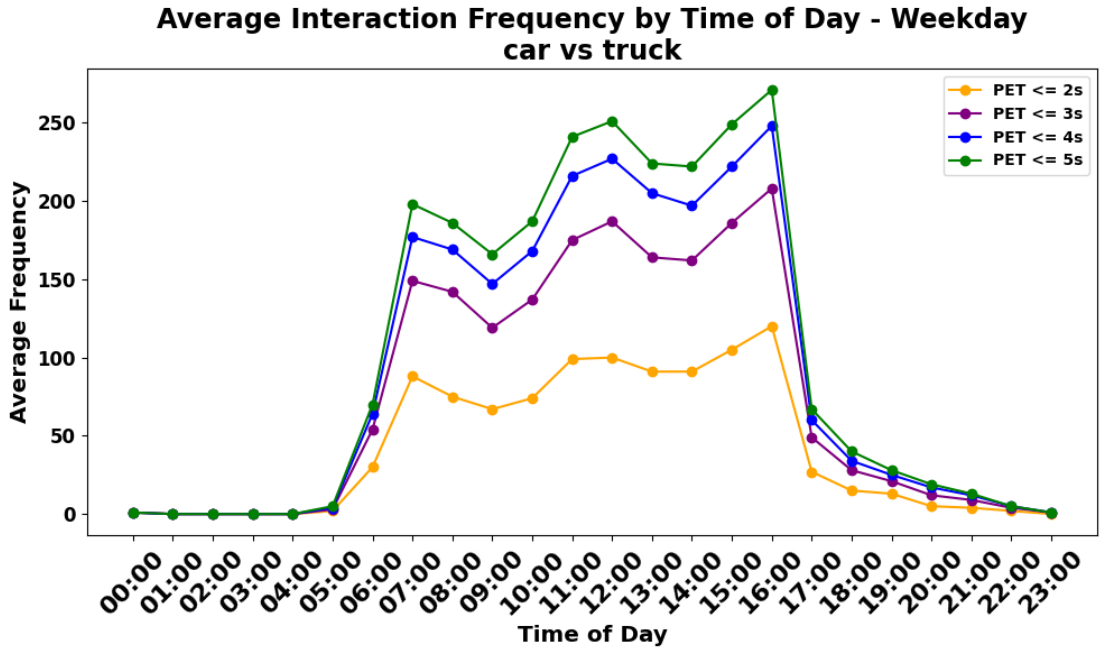

(a)

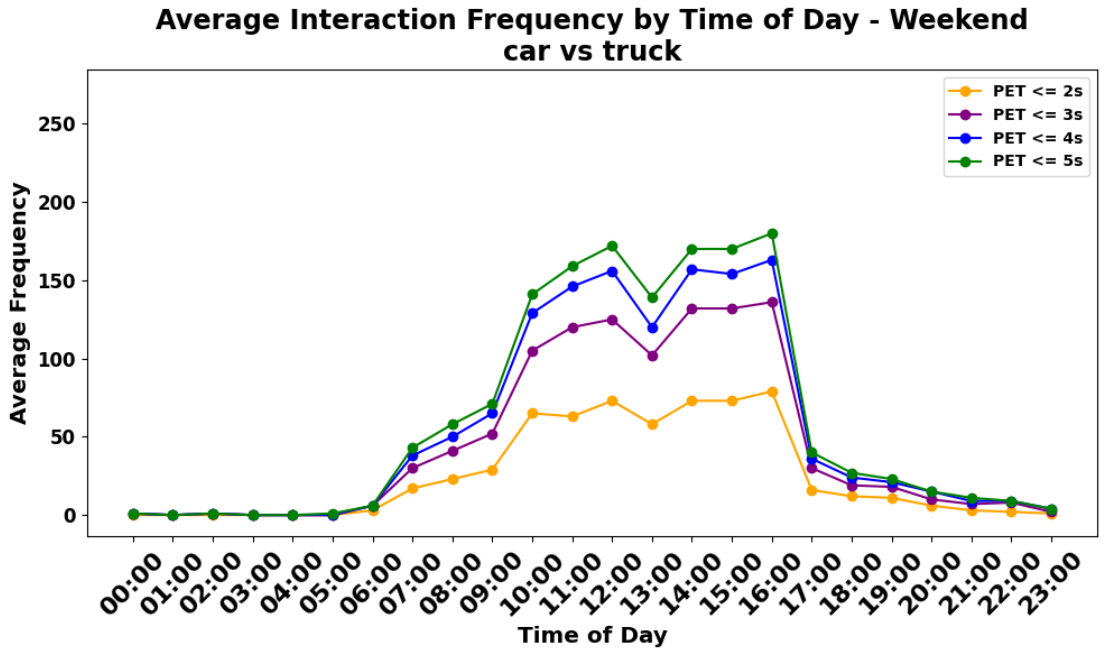

(b)

Figure 12. Graph. Average frequency of car vs. truck interactions by hour; (a) weekdays, (b) weekends.

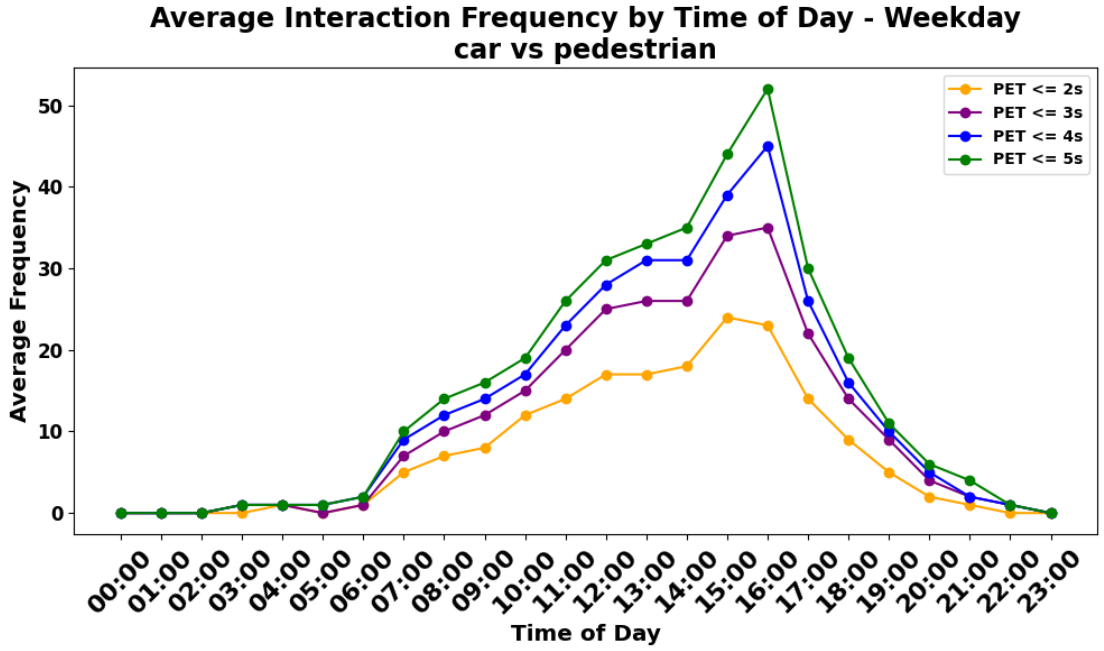

(a)

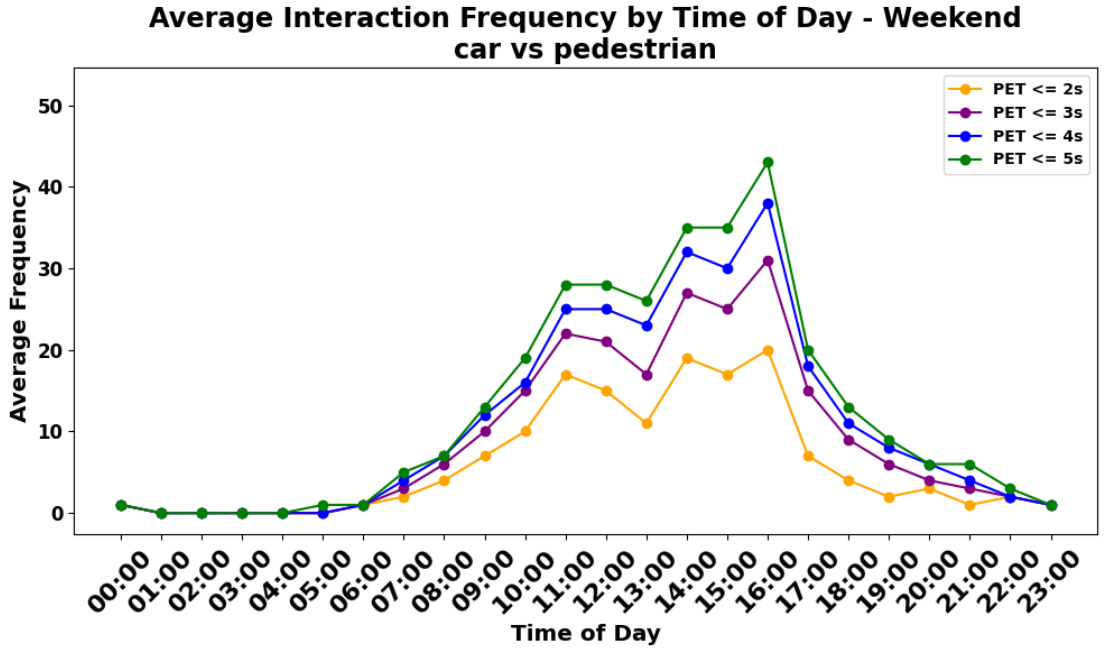

(b)

Figure 13. Graph. Average frequency of car vs. pedestrian interactions by hour; (a) weekdays (b) weekends.

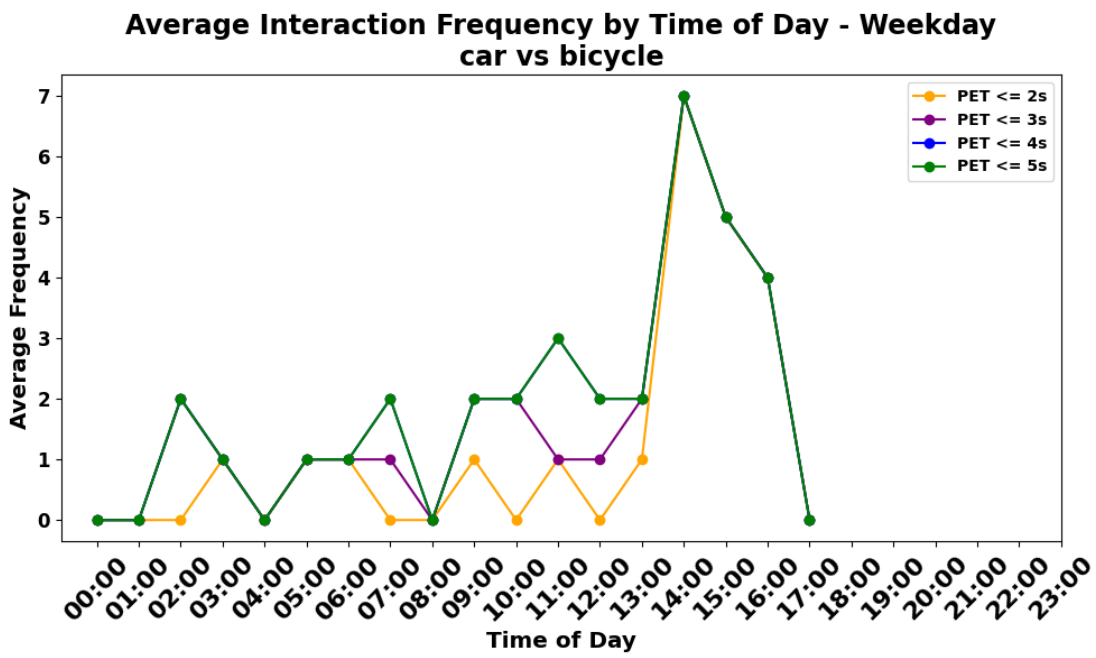

(a)

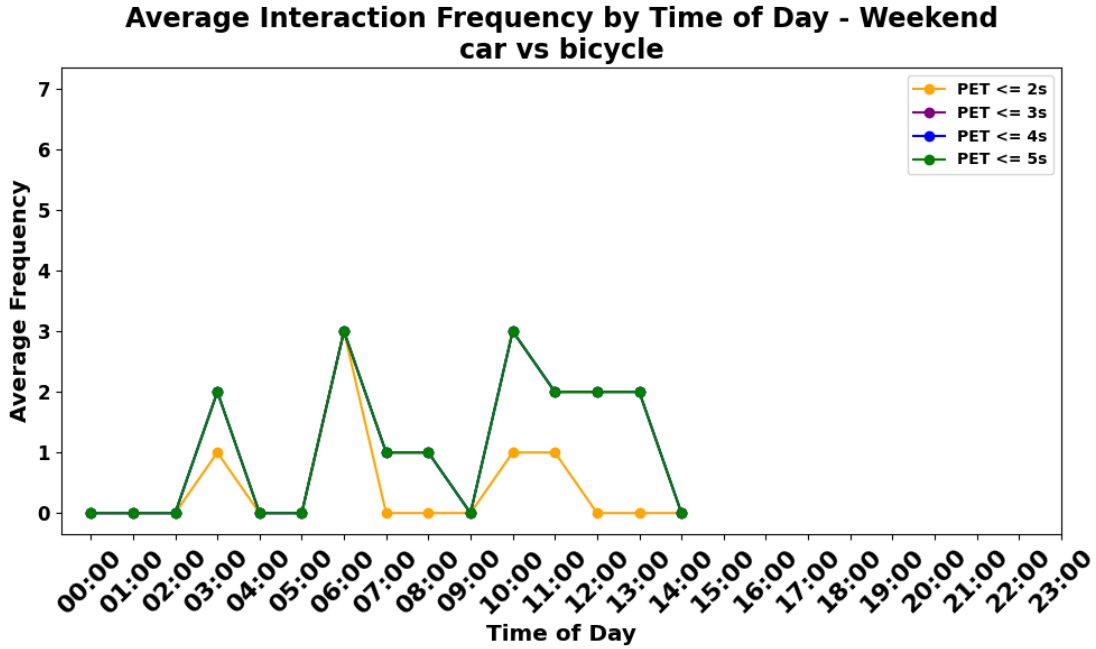

(b)

Figure 14. Graph. Average frequency of car vs. bicycle interactions by hour; (a) weekdays, (b) weekends.

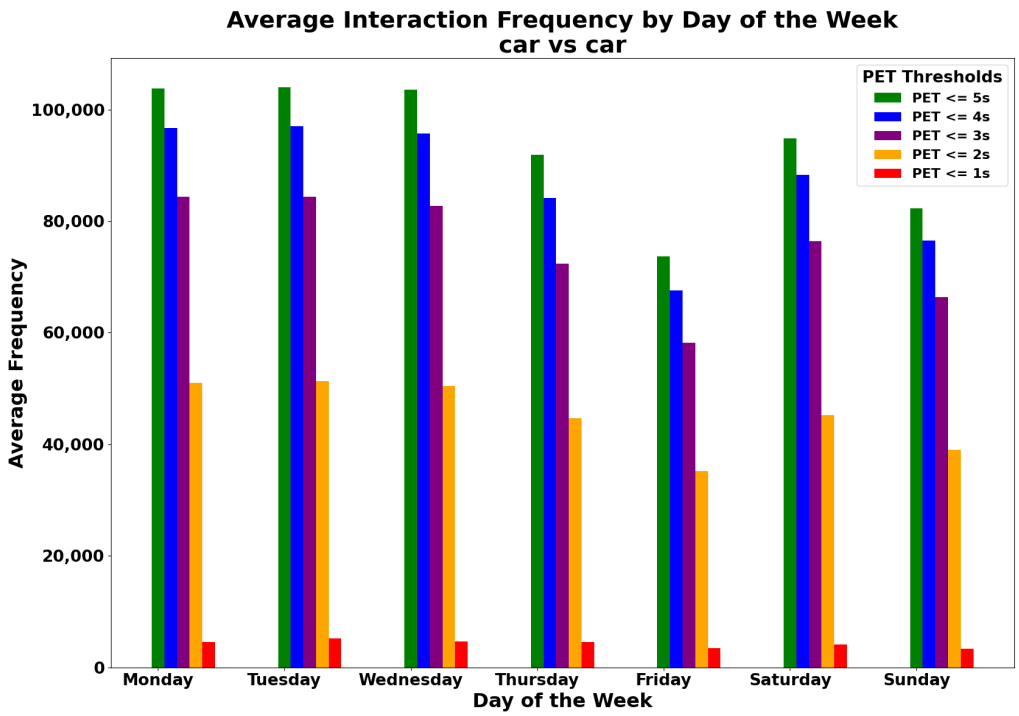

(a)

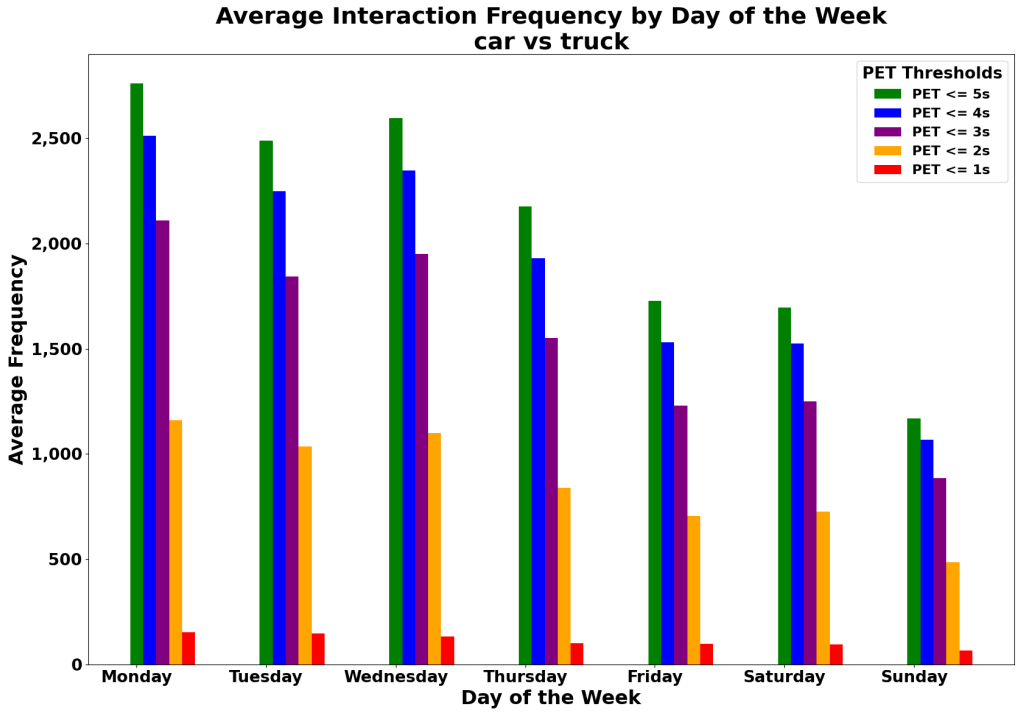

(b)

Figure 15. Graph. Average frequency of interactions per day; (a) car vs. car, and (b) car vs. truck.

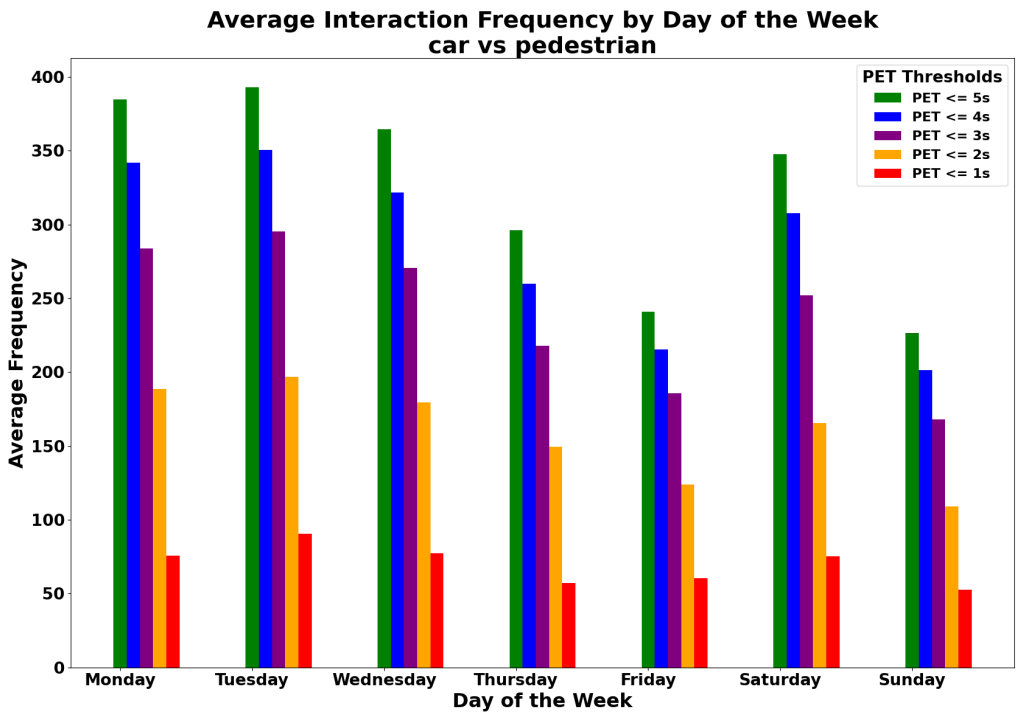

(a)

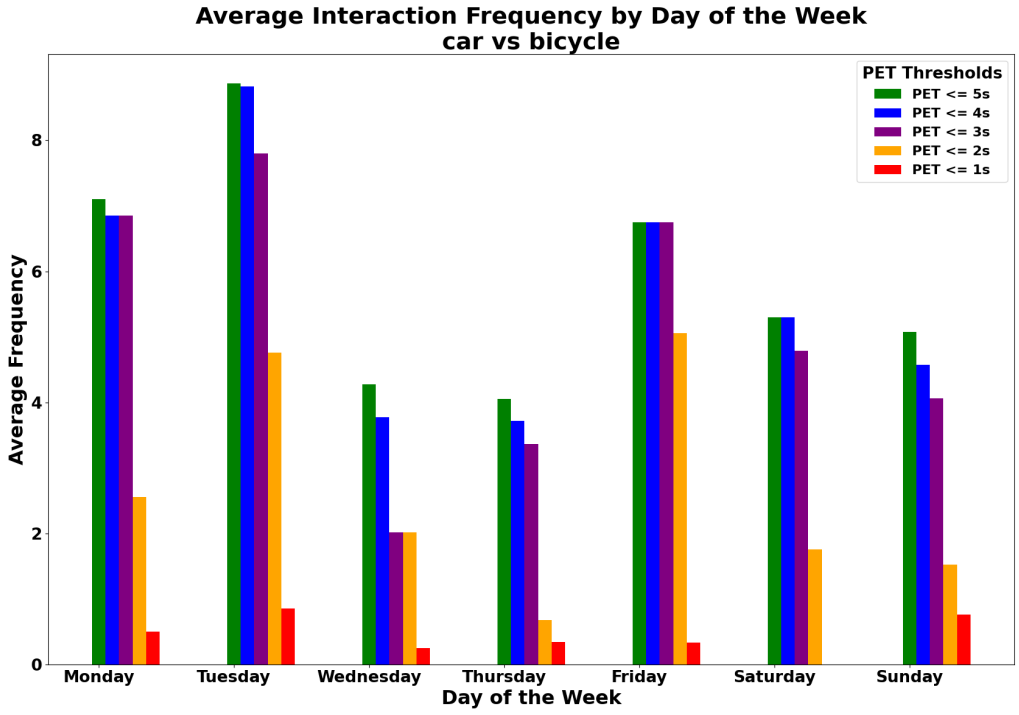

(b)

Figure 16. Graph. Average frequency of interactions per day; (a) car vs. pedestrian, and (b) car vs. bicycle.

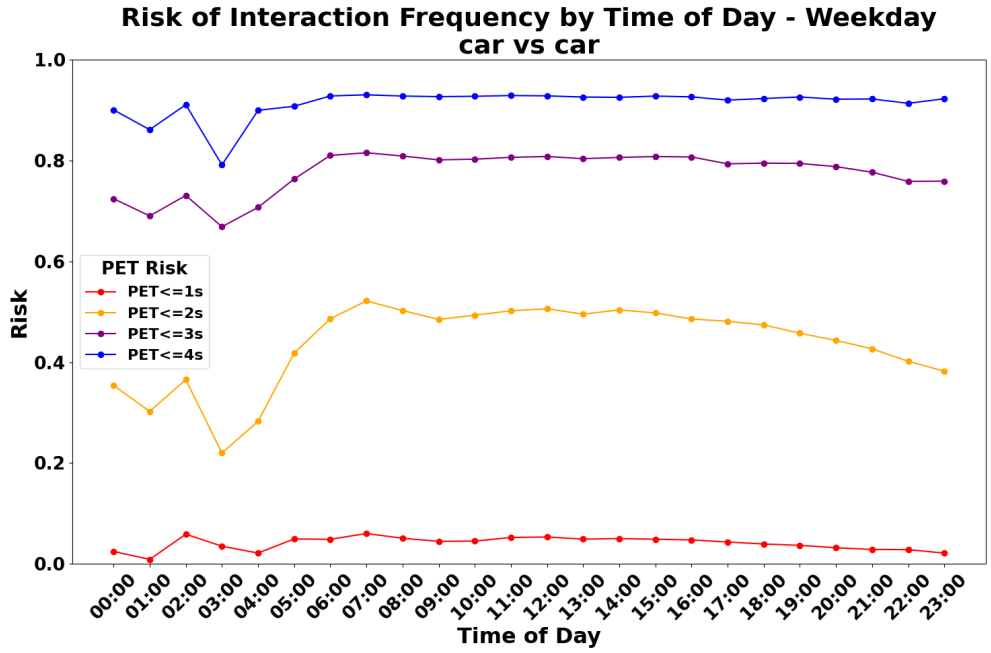

(a)

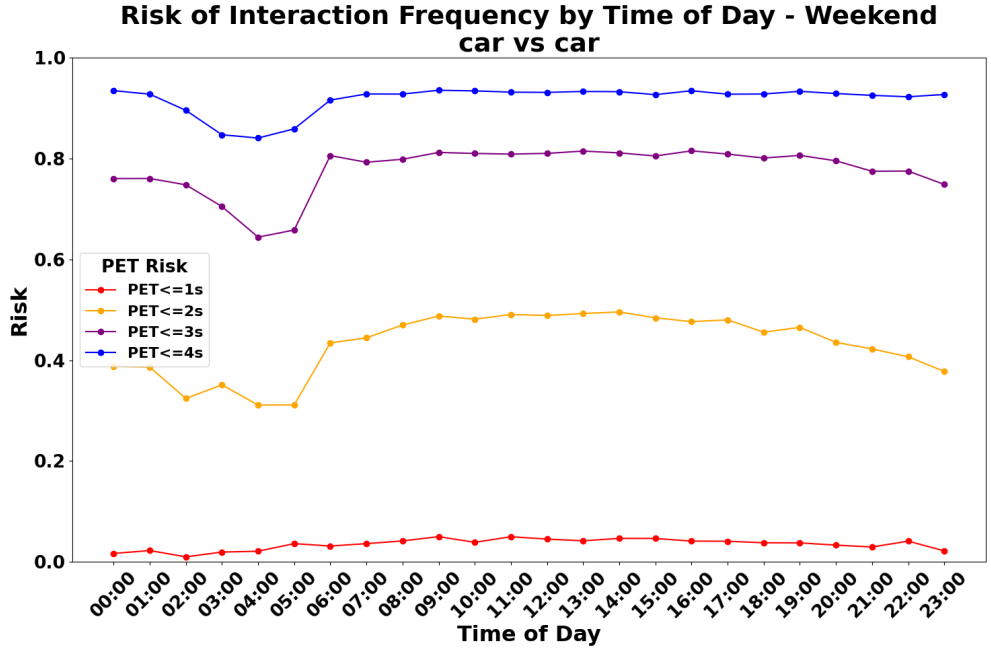

(b)

Figure 17. Graph. Risk of car vs. car near-crashes per hour during (a) weekdays, (b) weekends.

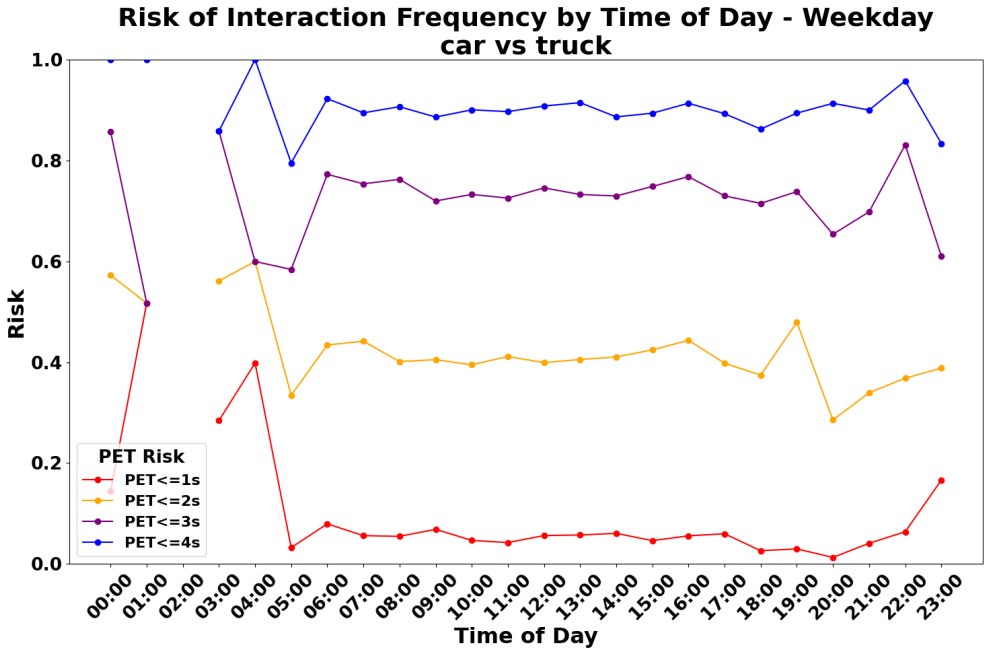

(a)

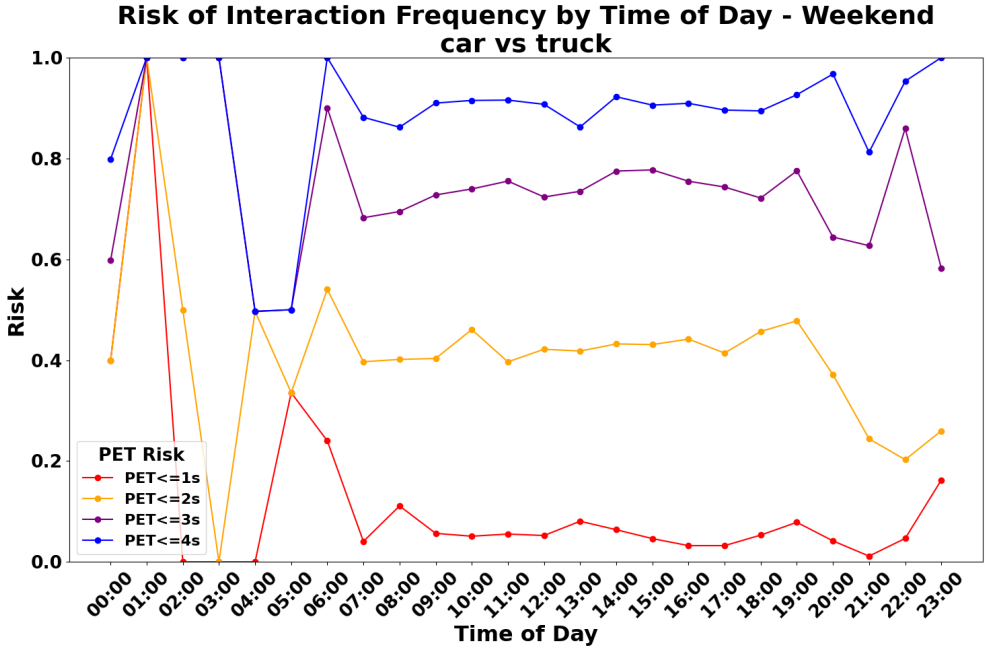

(b)

Figure 18. Graph. Risk of car vs. truck near-crashes per hour during (a) weekdays, (b) weekends.

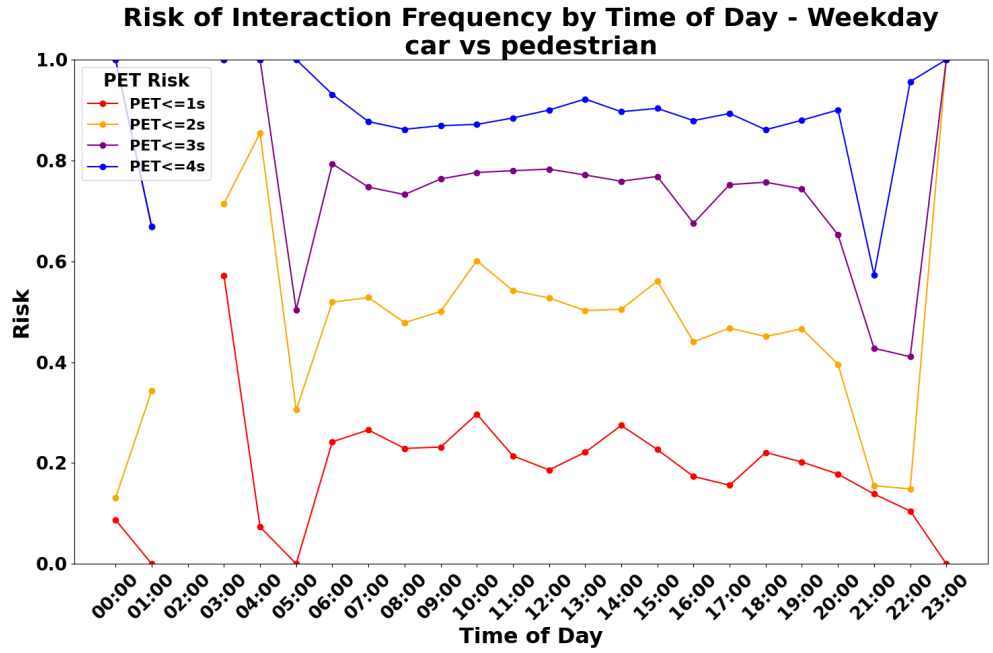

(a)

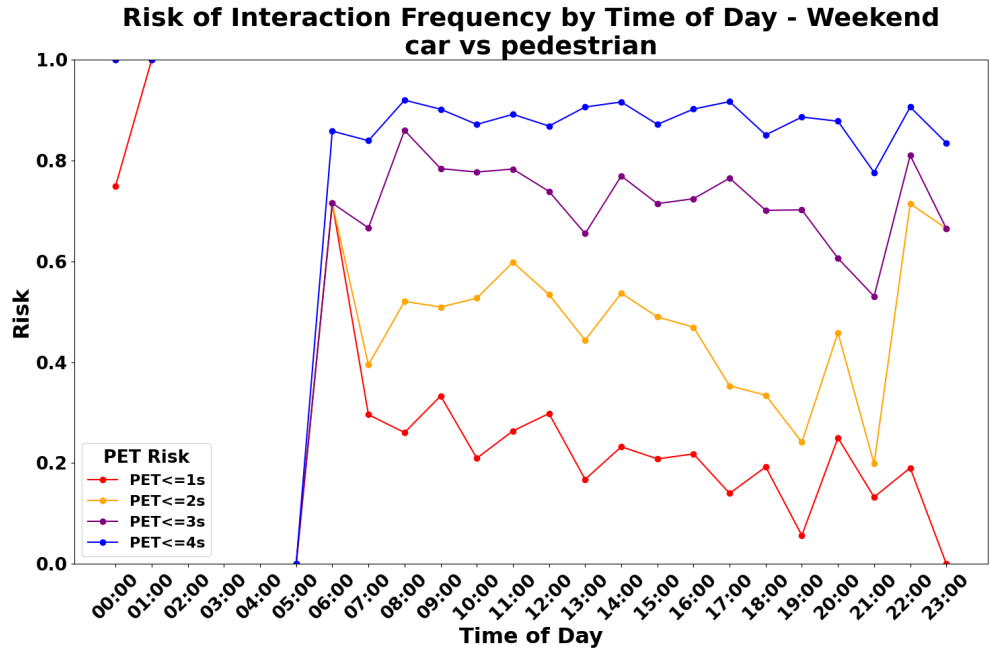

(b)

Figure 19. Graph. Risk of car vs. pedestrian near-crashes per hour during (a) weekdays, (b) weekends.

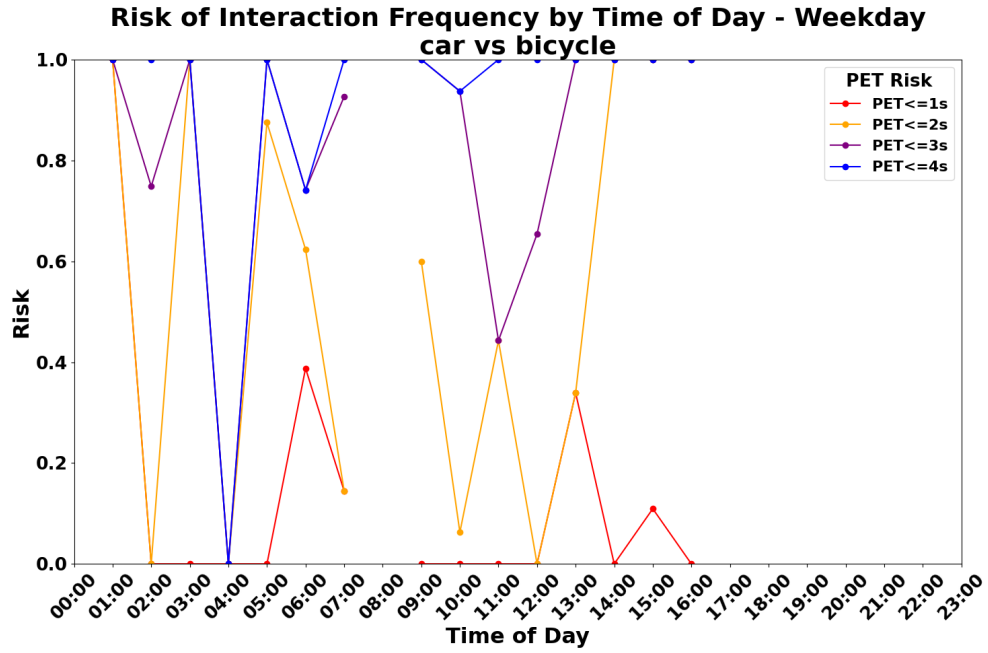

(a)

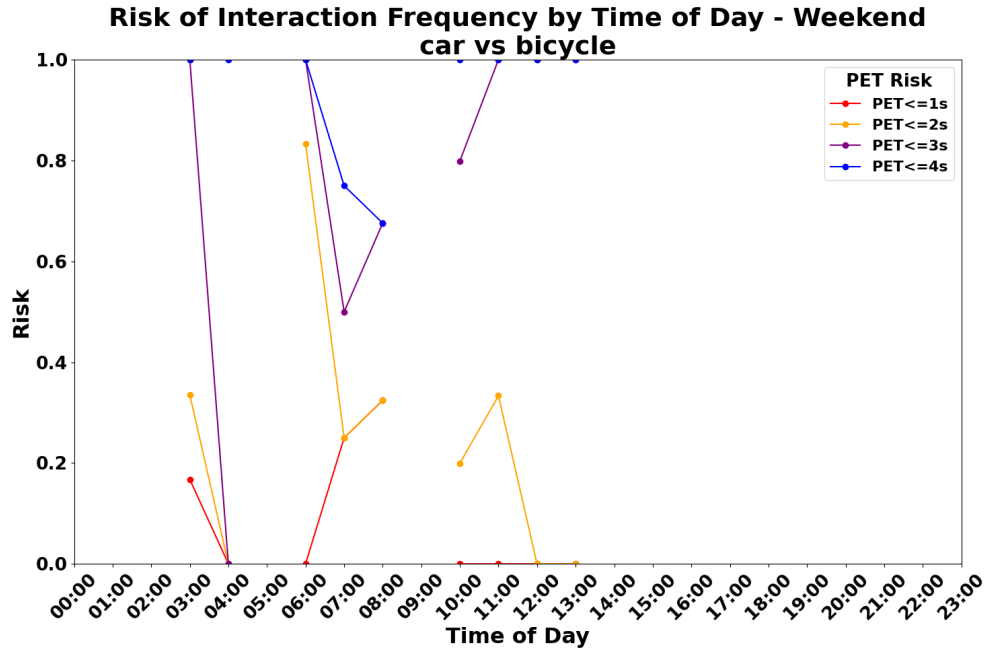

(b)

Figure 20. Graph. Risk of car vs. bicycle near-crashes per hour during (a) weekdays, (b) weekends.

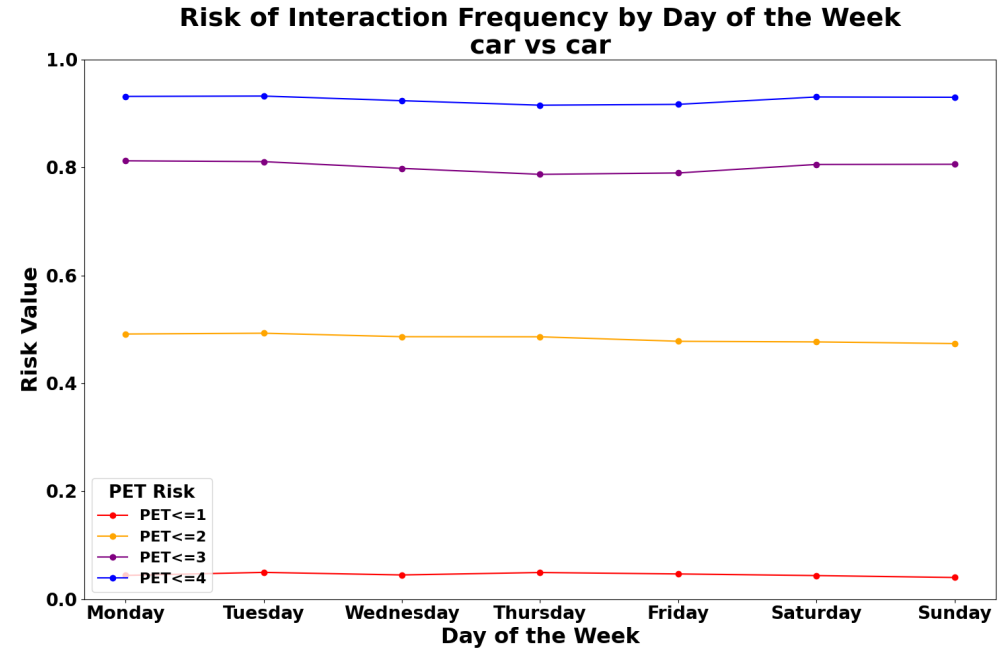

(a)

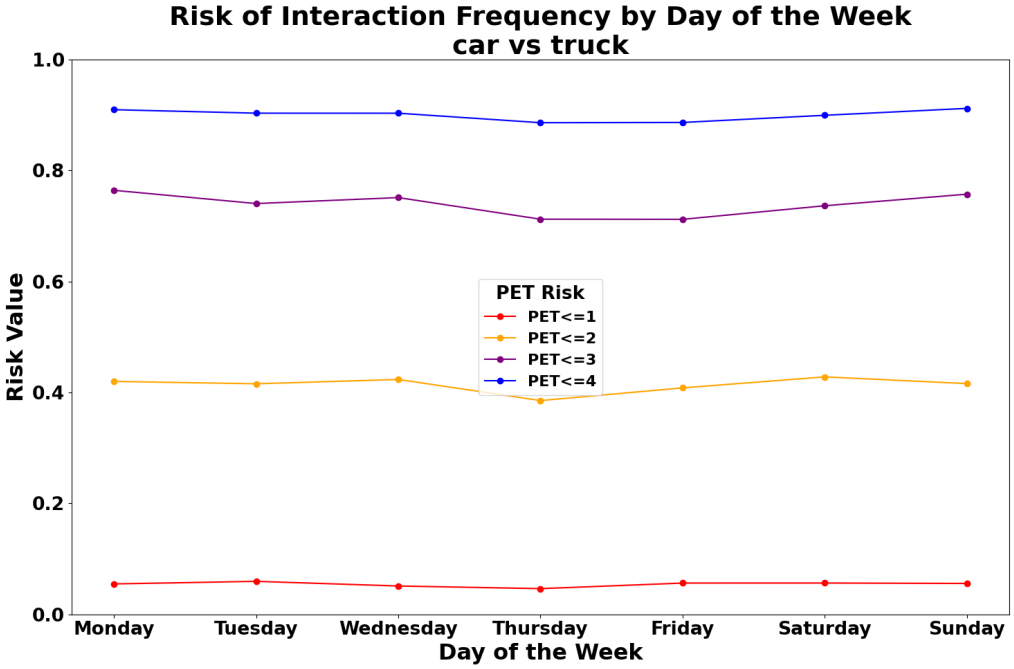

(b)

Figure 21. Graph. Risk of near-crashes over the week for (a) car-car, and (b) car-truck interactions.

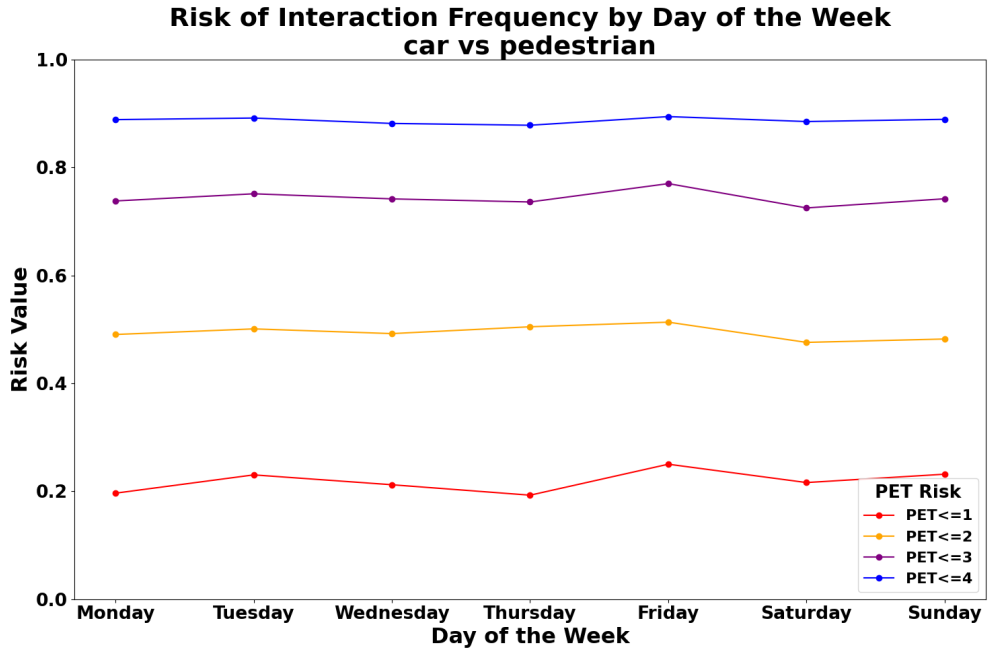

(a)

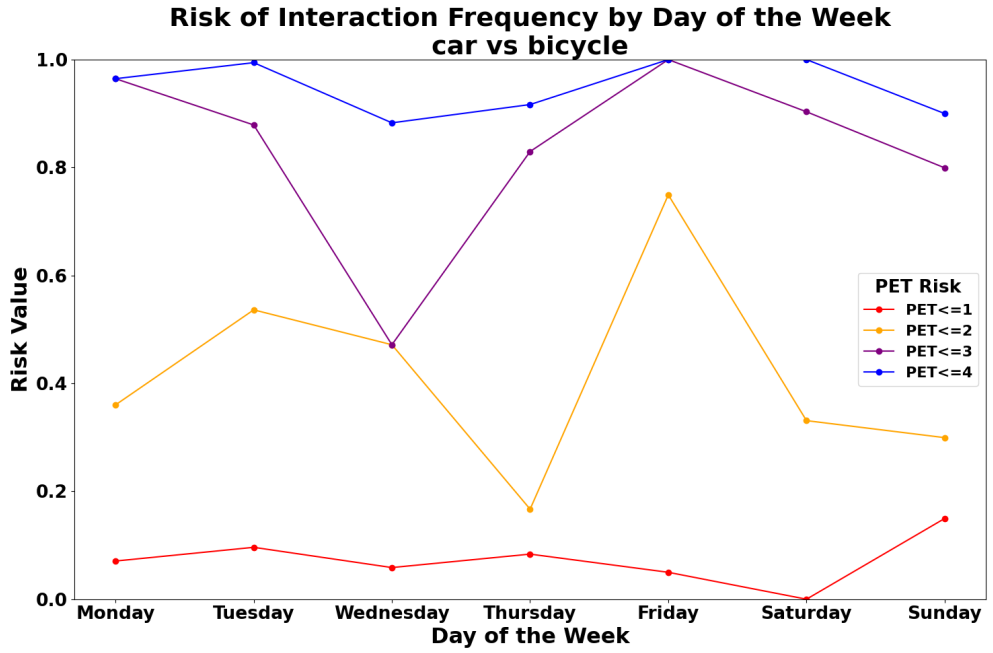

(b)

Figure 22. Graph. Risk of near-crashes over the week for (a) car-pedestrian, and (b) car-bike interactions.

Appendix D

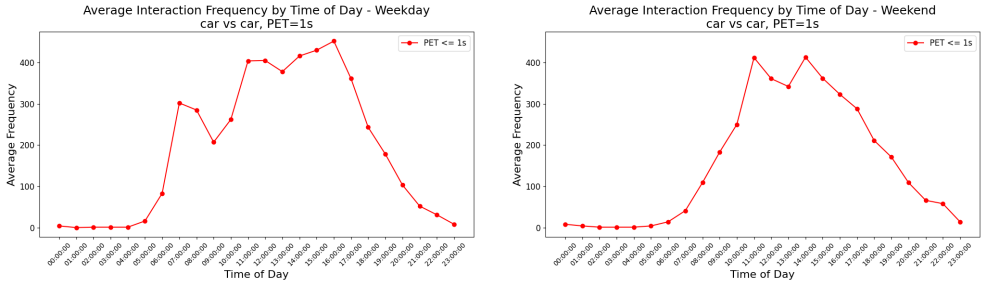

(a) (b)

Figure 23. Average frequency of most severe car vs. car interactions by hour; (a) weekdays, (b) weekends.

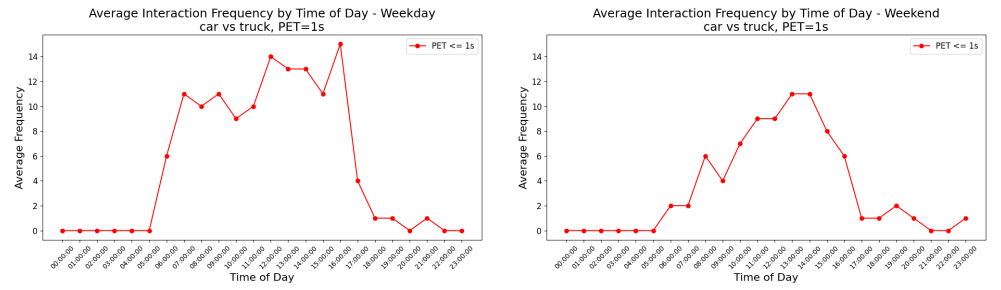

(a) (b)

Figure 24. Graph. Average frequency of most severe car vs. truck interactions by hour; (a) weekdays, (b) weekends.

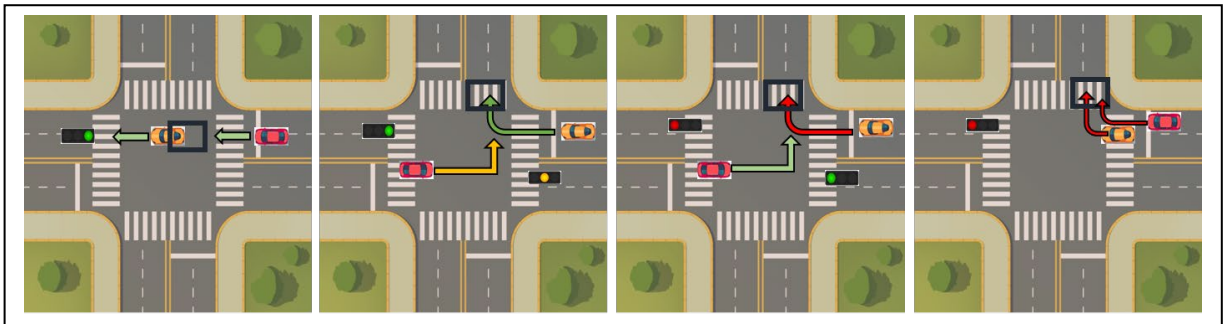

(a) (b) (c) (d)

Figure 25. Diagram. Near-crash events in different stage of the signal; (a) green-green, (b) green-yellow. (c) red-green, (d) red-red.

Appendix E

Table 3. Dashboard Panel

Volumes	PET Interactions
Total Volume by Mode	Average PET per Mode
Volume per Block	Interaction Severity Frequency Time Series
Movement Frequency Time Series	Interaction Severity Frequency
All Modes Frequency Time Series	Intersection PET Heatmap
	Normalized Heatmap
	Average PET per Block Status Over Time
	Average PET per Mode Status Over Time

Table 4. Dashboard Variables List

Variable	Description
Block	Allows users to select single, multiple, or all blocks found in the intersection
Interval	Allows users to choose time intervals for grouping visualized data
Mode1	Allows users to select single, multiple, or all modes of transportation
Mode2	Allows users to choose single, multiple, or all modes of transportation
VeryDangerousPET	Users can set their own threshold values for very dangerous interactions

Variable	Description
DangerousPET	Users can set their own threshold values for dangerous interactions
MildPET	Users can set their own threshold values for mild interactions
VeryDangerousPET_Weight*	Users can input their own weights for very dangerous interactions
DangerousPET_Weight*	Users can input their own weights for dangerous interactions
MildPET_Weight*	Users can input their own weights for mild interactions
noPET_Interaction	Users can input their threshold values for the no interactions
Street	Users can select the intended street name
Time	Users can set the time range for processing the data

** **The variables are used to give importance to each type of PET interaction (very dangerous, dangerous, and mild PET) for calculating the combined interaction frequency in the heatmap. This variable is solely referenced by the panel named Intersection PET Heatmap.***

The "Movement Frequency Time Series" panel is linked to the Street, Time, and Interval variables within the dashboard. When a specific street name is selected, this panel provides a visualization of movement frequency for various types (through movement, left turn, right turn) within the chosen time frame and selected interval. For instance, Figure 27 illustrates the movement frequency on "H St West" over time, utilizing a 15-minute interval for reference.

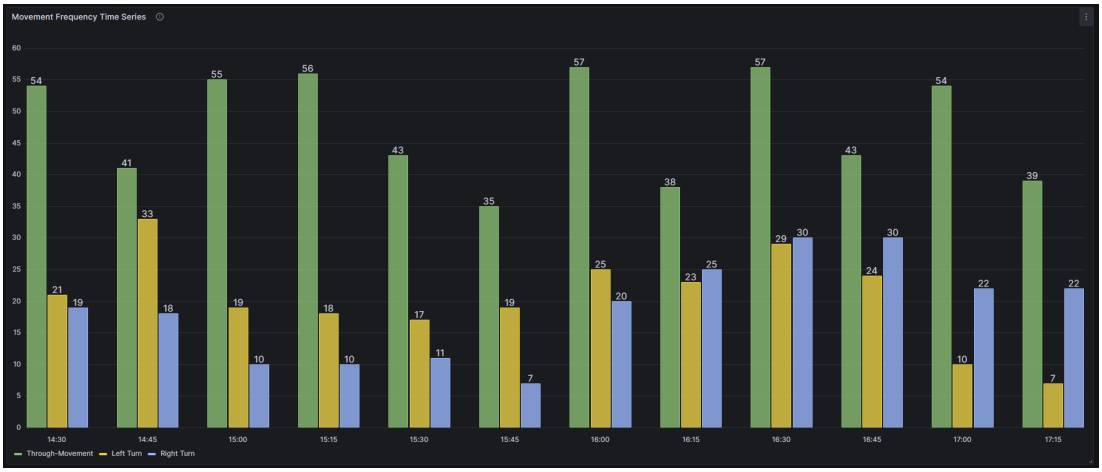

Figure 26. Screen capture. H Street West Movement Frequency Time Series Panel.

The “All Modes Frequency Time Series” panel is connected to the Time and Interval variables within the dashboard. As an example, Figure 28 presents the combined frequency of all transportation modes over a specified time period and the chosen interval. Figure 28(a) showcases the volume during the a.m. peak hour, while Figure 28(b) illustrates the volume during the p.m. peak hour, with both using a 15-minute interval.

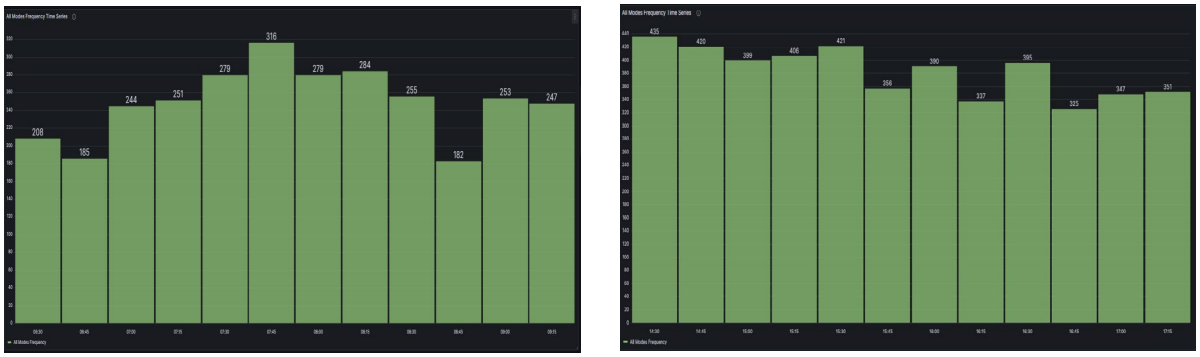

(a) **(b)**

Figure 27. Screen capture. All Modes Frequency Time Series Panel; (a) AM peak hour, (b) PM peak hour.

The “Average PET per Mode Status” panel relies on the Mode1, noPET_interaction, and Time variables within the dashboard. Once these variables are provided, the panel calculates and displays the average PET values for the selected mode1 in conjunction with all other modes (Car, Truck, Motorcycle, Bicycle, Bus, Pedestrian) where the PET values are less than the specified noPET_interaction threshold over the chosen time period. As illustrated in Figure 29, this panel is configured with Mode1 set to “Car” and a noPET_interaction threshold of 5 s, enabling the assessment of average PET values for car interactions with other modes meeting the defined criteria.

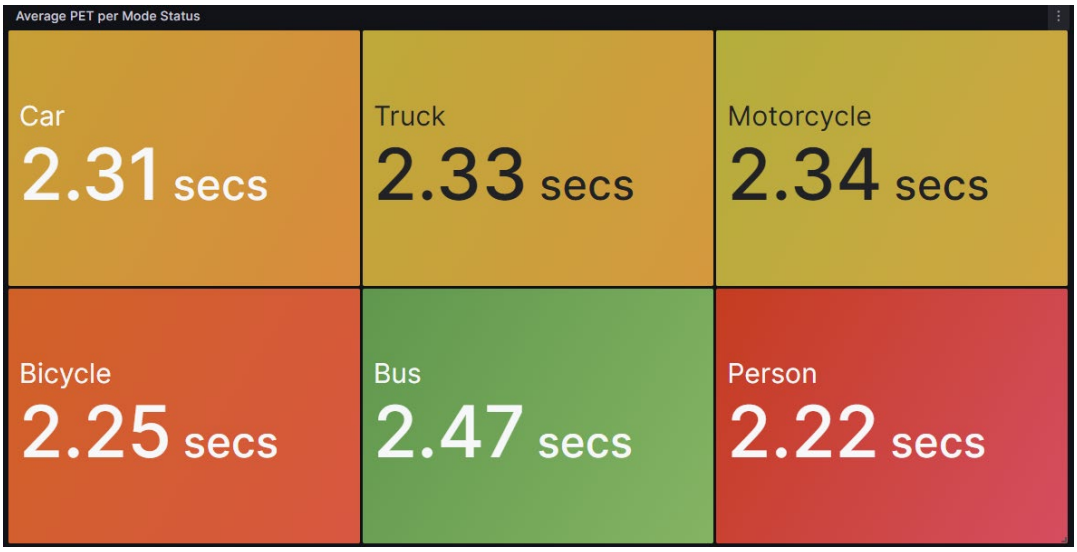

Figure 28. Screen capture. Average PET per Mode Status Panel.

The "Interaction Severity Frequency" panel references the verydangerousPET, dangerousPET, and mildPET dashboard variables. It determines the frequency of the varying PET interactions based on comparing the PETs per mode against the PET dashboard variables' threshold values determined by the user for a specified time range. Then it displays these values in a vertical bar gauge format, shown in Figure 30. Figure 31, on the other hand, represents the "Interaction Severity Frequency Time Series" panel, which allows users to analyze the frequency of interaction severity over a specific time range using a user-defined interval value, with a 15-minute interval shown in this chart.

Figure 29. Screen capture. Interaction Severity Frequency Panel.

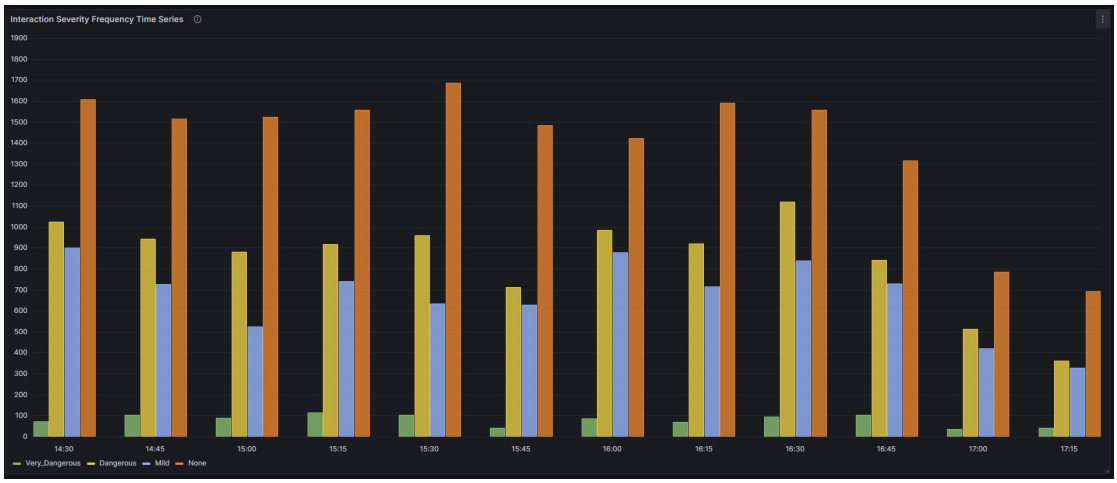

Figure 30. Screen capture. Interaction Severity Frequency Time Series Panel.

Appendix F

Table 5 Data Specification

Variable	Description
ID1	Identifier for the first object involved in the interaction.
ID2	Identifier for the second object involved in the interaction.
Mode1	Mode or type of the first object involved in the interaction.
Mode2	Mode or type of the second object involved in the interaction.
Line1_PET	ID of the white (as shown in the demo) line crossed by the first object in the interaction.
Line2_PET	ID of the white (as shown in the demo) line crossed by the second object in the interaction.
Time1	Time at which the first object crosses the line of the drawn block in the intersection.
Time2	Time at which the second object crosses the line of the drawn block in the intersection.
PET	Time difference (in seconds) between Time2 and Time1.
Interaction	Severity type of the interaction based on predefined thresholds (e.g., “No Interaction,” “Mild Interaction,” “Dangerous Interaction,” “Very Dangerous Interaction”).
Mode_ID1	Mode or type of the first object involved in the interaction.
Line1_ID1	ID of the first blue (as shown in the demo) line crossed by the first object.
Line2_ID1	ID of the second blue (as shown in the demo) line crossed by the first object.
To_ID1	Street destination name of the first object.
Movement_ID1	Type of movement for the first object (e.g., “Through movement,” “Right Turn,” “Left Turn”).
Mode_ID2	Mode or type of the second object involved in the interaction.

Variable	Description
Line1_ID2	ID of the first blue (as shown in the demo) line crossed by the second object.
From_ID1	Street origin name of the first object.
Line2_ID2	ID of the second blue (as shown in the demo) line crossed by the second object.
From_ID2	Street origin name of the second object.
To_ID2	Street destination name of the second object.
Movement_ID2	Type of movement for the second object (e.g., “Through movement,” “Right Turn,” “Left Turn”).
Camera	Camera ID that captured the objects (possible values: 8005, 8006, 8007, 8008).